Metallomics, 15, 2023, mfad051
https://doi.org/10.1093/mtomcs/mfad051
Advance access publication date: 2 September 2023
Paper

Wilson disease–causing mutations in the carboxyl terminus of ATP7B regulates its localization and Golgi exit selectively in the unpolarized cells

Kaustav Chakraborty[1], Santanu Das[2,‡], Anusree Pal[1], Saptarshi Maji[2], Bhawana Rai[1], Arnab Gupta[2] and Ashima Bhattacharjee[1,*]

[1]Amity Institute of Biotechnology, Amity University, Kolkata, India and [2]Department of Biological Sciences, Indian Institute of Science Education and Research, Kolkata, India
*__Correspondence__: Ashima Bhattacharjee, Amity University Kolkata, Plot nos. 36, 37 and 38, Major Arterial Road, Action area II, Kadampukur Village, Rajarhat, Newtown, West Bengal—700135, India. E-mail: abhattacharjee@kol.amity.edu
‡Current affiliation: Department of Pathology and Laboratory Medicine, Children's Hospital of Philadelphia, PA, USA.

Abstract

Mutational inactivation of the P-type Cu-ATPase ATP7B interferes with its cellular functions to varying extent leading to varied cellular phenotypes. Wilson's disease (WD) primarily affects organs composed of polarized/differentiated epithelial cells. Therefore, phenotypic variability might differ depending on the polarization/differentiation of the cells. The present study investigates the intracellular stability and localization of ATP7B harboring WD mutations in both unpolarized/undifferentiated and polarized/differentiated cell-based models. Green fluorescent protein (GFP)-ATP7B harboring the WD causing mutations, N41S, S653Y, R778Q, G1061E, H1069Q, S1423N, S1426I, and T1434M, are included for investigation. The C-terminal WD mutations (S1423N, S1426I, and T1434M), exhibit distinct localization and Cu(I) responsive anterograde and retrograde trafficking in undifferentiated/unpolarized vs. differentiated/polarized cells. While basal localization of the S1423N mutant gets corrected in the differentiated glia, its Cu(I) responsive anterograde and retrograde trafficking behavior is not identical to the wild-type. But localization and trafficking properties are completely rescued for the S1426I and T1434M mutants in the differentiated cells. Comprehensive meta-analysis on the effect of the reported C-terminal mutations on patient phenotype and cultured cells demonstrate discrete regions having distinct effects. While mutations in the proximal C-terminus affect ATP7B stability, the present study shows that the distal region dictates cell-specific Trans Golgi Network (TGN) localization and exit. The localization and export properties are corrected in the differentiated cells, which is a plausible mechanism for the milder phenotype exhibited by these mutations. It highlights the critical role of the C-terminus in cell-specific TGN retention and exit of ATP7B.

Keywords: ATP7B, differentiated glia, mutation, polarized, Wilson disease

Graphical abstract

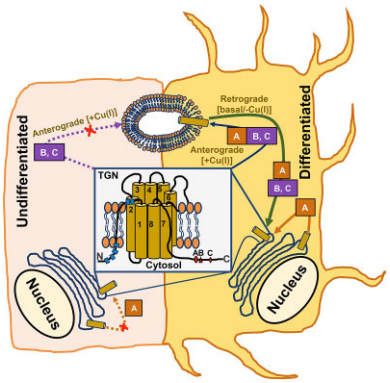

Rescue of the localization and trafficking properties of ATP7B bearing C-terminal mutations (S1423N, S1426I and T1434M) in the polarized/differentiated cells. S1423N (A) mutant fails to localize into the TGN in the undifferentiated C-6 cells. But the mutant localizes into the TGN and shows vesicular localization (anterograde trafficking) in response to $CuCl_2$ treatment in the C-6 derived glia. However, S1423N can partially traffic back to the TGN from the vesicles (retrograde trafficking) under Cu(I) limiting condition. S1426I (B) and T1434M (C) mutants localize on the TGN both in the undifferentiated and differentiated (glia) C-6 cells. However, the mutants fail to perform anterograde and retrograde trafficking in the undifferentiated cells but can do so in the differentiated glia.

Received: March 22, 2023. **Accepted:** August 6, 2023

Introduction

Copper Cu(I) is an essential micronutrient performing key role as cofactor for a spectrum of essential enzymes. But excess intracellular copper, arising from the disruption in the export pathway, adversely affects various intracellular processes leading to Wilson's disease (WD). WD is caused by the mutational inactivation of ATP7B, leading to the failure of the export of copper into the bile. The excess copper accumulates in the liver and other organs[1] including in brain and kidney. WD follows an autosomal recessive mode of inheritance. WD exhibits a wide spectrum of phenotypic heterogeneity despite being a monogenic disorder. Lack of any established modifiers for the disease or involvement of other candidates makes the understanding of such variability quite incomplete. Heterogeneity, in the phenotype, is manifested both in the hepatic and neurological manifestations.

ATP7B is a 165 kDa protein with multiple cytosolic domains and eight transmembrane segments.[2,3] Copper transport by the ATPase depends on its changes in conformation dictated by phosphorylation and dephosphorylation[3] and interdomain interaction. The effects of the missense mutations on the protein can be varied. Variability can be in the stability, domain functions, or interdomain contacts. Also, effects of the mutations on the local or global conformation can be variable, which, in turn, can be manifested into the variability of function. ATP7B is expressed in varied cell types including polarized cells such as the intestinal epithelium, hepatocytes, neurons, glia, etc. Each of these cells has their unique proteome related to their location and function. Therefore, it is probable that effects of the mutations on ATP7B can be different in the polarized vs. unpolarized cells and among various polarized cells. Therefore, effect of the mutations on the cellular properties of ATP7B demands the study of the effects of the individual mutations on protein structure, function, and cellular localization along with their investigation in various polarized/differentiated cell-based models.

In this study, we took an array of WD-causing mutations and studied their intracellular stability, Cu(I) transport capacity in the Trans Golgi Network (TGN) lumen, and ability to traffic to the vesicles in response to high intracellular copper. The WD mutations studied are N41S, S653Y, R778Q, G1061E, H1069Q, S1423N, S1426I, and T1434M (Supplementary Fig. S1).[4,5] Our results demonstrate correlation between the intracellular stability of the mutant ATP7B with its localization, Cu(I) transport capacity and copper-mediated vesicular localization. We report, for the first time, the differential ability to perform copper dependent anterograde and retrograde trafficking by the ATP7B-T1434M and ATP7B-S1426I in the differentiated glia and polarized Madin–Darby canine kidney (MDCK) cells compared to their undifferentiated/unpolarized counterparts. ATP7B-T1434M and ATP7B-S1426I can perform Cu(I) responsive anterograde and retrograde trafficking in the differentiated cells, but unable to do so in the undifferentiated/unpolarized cells. Both the mutants localize to the same vesicles as the wild-type (WT) in response to $CuCl_2$ treatment. Again, ATP7B harboring another C-terminal WD mutation, S1423N, fails to localize on the TGN in the undifferentiated C-6 cells under basal Cu(I) condition. But the mutant ATP7B can localize to the TGN, under basal condition, in the differentiated C-6 derived glia. However, the mutant does not localize to the same vesicles as the WT protein in response to $CuCl_2$ treatment and consequently can partially retrieve back to the TGN in response to low intracellular Cu(I). Meta-analysis on the effect of the C-terminal WD mutations in ATP7B reveals a nice correlation on the location of the mutation with their nature of cellular effects. This in turn shows a relevant correlation with the patient phenotypes in certain cases.

Materials and methods

Cell culture, differentiation, and polarization

HEK293T, C6 (rat glioma), and YS (Menkes disease fibroblast was a generous gift from Prof. Svetlana Lutsenko, Johns Hopkins School of Medicine, USA). Cells were maintained in Dulbecco's modified Eagle medium (DMEM—high glucose, Gibco) containing 10% fetal bovine serum (heat inactivated, HiMedia), 1% penicillin–streptomycin (HiMedia), and 1% amphotericin B (Gibco) at 37°C and 5% CO_2. Differentiation of C6 was initiated as reported.[6] Briefly, undifferentiated C6 (1×10^5) cells were plated on a 35 mm dish or six-well plates and allowed to grow in complete media for 48 h. After that, cells were rinsed twice with 1X phosphate buffered saline (PBS; Gibco) and kept in a medium without serum for 1 h. After transfection, differentiation was initiated by the addition of 500 μM dBcAMP (N6,2′-O-di-butyryl adenosine 3′,5′-cyclic monophosphate sodium salt, Sigma-Aldrich) and 1 mM theophylline (MP Biomedicals) in medium (DMEM with 1% Pen-Strep and 1% Amphotericin B) without serum. Differentiation was carried out for 24 h.

MDCK-II line was grown and polarized as per reported.[7] Briefly, cells were maintained in a complete medium of DMEM (high glucose, Sigma-Aldrich) supplemented with 10% fetal bovine serum (Gibco), 1% penicillin–streptomycin (Gibco), and 1% amphotericin B (Gibco). Cells were grown in Trans-well plates (Corning) and allowed to grow for 3 to 4 days for polarization.

Plasmids, generation of WD mutant, and transfection

The plasmid pYG7 encoding full-length WT ATP7B with an N-terminus green fluorescent protein (GFP) has been used.[8] WD-causing mutations are introduced by using the QuickChange XL site-directed mutagenesis kit (Agilent Technologies) and Q5 Site-Directed Mutagenesis Kit (New England Biolabs) utilizing the GFP-ATP7B with the use of suitable primers (Supplementary Table S1). ATP7B harboring the H1069Q[8] and S1423N[7] has been used as reported. The different mutant forms of GFP-ATP7B were further verified by sequencing the entire cDNA region (Supplementary Fig. S2).

For the transient transfection of HEK293T and C6, cells were grown on a six-well plate, 1.5 and 2.5 μg of plasmid DNA, respectively, have been used. Either WT GFP-ATP7B or the plasmids bearing the ATP7B mutation (N41S, S653Y, R778Q, G1061E, H1069Q, S1423N, S1426I, T1434M) was transfected by using the Lipofectamine 3000 reagent (Thermo Fisher Scientific) according to manufacturer's protocol with slight modifications. C-6 cells are differentiated following transfection, into glia, as described earlier. For, the tyrosinase assay, the YS cells were co-transfected either with 2 μg WT tyrosinase plasmid (pEGFPn1 with WT-Tyr, gift from Prof. Kunal Ray, Ramakrishna Mission Vivekananda Educational and Research Institute, West Bengal, India) and 2 μg of either WT or mutant plasmid by using lipofectamine 3000. Transfection was performed according to manufacturer's protocol. After 6 h, the media were replaced with fetal bovine serum (FBS) containing DMEM complete media and kept for 16–18 h.

For transfection in MDCK, cells were nucleofected using Nucleofector 2b Device, program T-23 (Lonza) in electroporation cuvettes (BTX) and after transfection, they were grown on Transwell (Corning) for 3–4 days or until attaining the polarized condition.

For studying copper-dictated trafficking of GFP tagged ATP7B in C6 cells (undifferentiated and differentiated), MDCK cells (unpolarized and polarized), and HEK293T, the cells were treated with either 50 or 100 μM copper chloride for 2 h before harvest.

For studying the retrograde trafficking of ATP7B, the transfected and differentiated C-6 cells and transfected HEK293T cells were treated with 50 μM $CuCl_2$ for 2 h followed by washing twice with 1X PBS followed by treatment with either 30 μM (ATP7B-R778Q), 50 μM (ATP7B-T1434M), or 70 μM (ATP7B-S1423N, ATP7B—S1426I) TTM (ammonium tetrathiomolybdate) for 2 h. Cells are harvested for immunostaining.

Generation of mKO2-ATP7B (WT) construct

The mKO2-HA-ATP7A is utilized to generate the construct. ATP7B is cloned in place of HA-ATP7A using MluI and NotI restriction sites to generate the mKO2-ATP7B construct. The primers used have been presented (Supplementary Table S1).

Cell lysis and Western blot

Transfected and untransfected cells (UT) were washed with ice-cold PBS (Gibco). Cell pellets were suspended in lysis buffer [PBS containing 1 mM ethylenediaminetetraacetic acid (EDTA), 1 mM of ethylene glycol tetraacetic acid (EGTA), 250 mM of sucrose, and protease inhibitor cocktail (GCC Biotech Pvt. Ltd.)] and kept on ice for 45 min with occasional mixing. Cells were ruptured by a Dounce homogenizer with 120 strokes of the loose pestle and 220 strokes of a tight pestle. The Lysate was centrifuged at 600 $\times g$ for 10 min at 4°C to remove the intact nucleus, cell debris, and unlysed cells (step 1). The supernatant was collected and centrifuged at 3000 $\times g$ for 30 min (step 2). The supernatant from step 2 was centrifuged at 20 000 $\times g$ for 30 min at 4°C to collect the microsome. The pellet is collected and solubilized into a membrane solubilizing buffer (PBS containing 1 mM of EDTA, 2.5 mM of sucrose, 0.1% of NP40, and 0.2% of Triton X 100) containing a protease inhibitor cocktail. The total protein was measured by Bradford (Sigma-Aldrich) assay. A total of 30 μg of protein-containing lysate was mixed with gel loading dye (2% SDS, 2.5% ß mercapto-ethanol, 7.5% glycerol, 2 M urea, and 0.005% bromophenol blue) and boiled at 70°C for 10 min. The lysates were then kept at room temperature and resolved in 6% denaturing SDS-PAGE. The proteins were transferred into a nitrocellulose membrane (Nitrocellulose Membrane, Roll, 0.45 μm, 30 cm × 3.5 m, Bio-Rad) at a constant current of 180 mA for 120 min at 4°C. The membrane was blocked with 3% BSA containing Tris-buffered saline (TBS) (pH-7.4) for 1 h at room temperature. After the blocking, the membrane is incubated overnight either with the anti-GFP antibody (Abcam, dilution 1:15 000) or anti-alpha 1 sodium potassium ATPase antibody (Abcam, dilution 1:3000) in 1% BSA containing Tris-buffered saline with 0.1% Tween 20 at 4°C. The membrane was washed thrice with TBS at 5 min intervals and again thrice with TBS with 0.1% Tween 20 (TBST) at the interval of 5 min. The membrane was incubated, for 2 h, either with goat anti-rabbit horseradish peroxidase (HRP) conjugated secondary antibody (Santa Cruz Biotechnology, dilution 1:10 000) or anti-mouse HRP conjugated secondary antibody (Santa Cruz Biotechnology, dilution 1:10 000) in 1% BSA containing TBST at room temperature. The membrane was washed thrice with TBST and thrice with TBS at 5 min intervals. Chemiluminescence is detected by adding ECL Substrate (Clarity Max Western ECL Substrate, Bio-Rad) using a chemidoc imaging system. (Chemi Doc Imaging System, Bio-Rad).

Immunocytochemistry

HEK293T and C6 cells (differentiated and undifferentiated) cells were plated on sterile coverslips placed onto each well either on 6- or 12-well plates. After transfection and respective $CuCl_2$ and TTM treatment, cells were washed with ice-cold PBS twice at 3 min time intervals. Cells were fixed with ice-cold 4% paraformaldehyde for 3 min, followed by permeabilization with chilled methanol for 1 min. In the last step, cells were kept in ice-cold methanol for 5 min. Each of the steps has been performed on ice. Cells are then washed with PBS twice at 3 min interval. For HEK293T cells, post washing with PBS, cell is permeabilized by incubating in 0.5% (v/v) TritonX-100 in PBS for 15 min at room temperature. Both C6 and HEK293T cells were blocked by 3% BSA containing PBS for 2 h at room temperature, followed by the addition of the primary antibody overnight. The primary antibodies are [anti-alpha 1 sodium potassium ATPase antibody (Abcam, 1:600 dilution), rabbit anti-calnexin antibody (Abcam, 1:500 dilution), mouse monoclonal TGN38 antibody (Novus Biologicals, 1:400 dilution), mouse monoclonal Golgin97antibody (Thermo Fisher Scientific, 1:400 dilution)] in 1% BSA containing PBST (phosphate buffered saline, pH-7.4 containing 0.1% Tween20. After that, coverslips are washed thrice with PBST at the interval of 10 min each. Coverslips are incubated with the respective secondary antibodies. The secondary antibodies are [goat anti-rabbit Alexa Flour 488 (Abcam, dilution 1:2000), donkey anti-mouse Alexa Fluor 568 (Thermo Fisher Scientific, 1:2000)] in PBST for 1.5 h at room temperature followed by washing with PBST (three times at 10 min interval) and PBS (3 times at 10 min interval), Coverslips were then mounted with either Fluoroshield mounting medium (Sigma-Aldrich, containing DAPI) or ProLong Gold Antifade Mountant (Thermo Fisher Scientific, without DAPI) and imaged with a confocal microscope (SP8 Lightening confocal microscope, Leica Microsystems and FV1000 confocal laser scanning microscope, Olympus). All images were acquired using either an oil immersion 63× or 100× objective lens and for C6 cells images were deconvoluted using Leica application suite X Lightning software (Leica Microsystems).

For MDCK cells, unpolarized cells on a coverslip or polarized cells on a trans-well plate were washed with ice-cold PBS (pH 7.4) twice at an interval of 3 min. The cells were fixed with 2% paraformaldehyde for 20 min at room temperature followed by quenching with 50 mM ammonium chloride for another 20 min at room temperature. Coverslips are subsequently washed with 1X PBS three times. After fixation, permeabilization and blocking are done with 1% BSA in PBS containing 0.075% saponin (PBS-S) for 20 min at room temperature followed by the addition of primary antibodies. The primary antibodies are mouse anti-Golgin 97 (Thermo Fisher Scientific, 1:400 dilution), mouse anti-sodium potassium ATPase (Abcam, 1:400 dilution), mouse anti-GP135 (Developmental Studies Hybridoma Bank—DSHB, 1:400 dilution). Primary antibody is diluted in 1% BSA containing PBSS and kept at room temperature in a moist chamber for 2 h. After 2 h of incubation, cells are washed with PBS-S three times and incubated with the corresponding secondary antibodies. The secondary antibody and their respective dilution are donkey anti-mouse IgG Alexa Fluor (Thermo Fisher Scientific, 1:2000 dilution) for 1.3 h at RT. This was followed by further washing with PBS-S three times and finally with PBS twice, Alexa Fluor 647 phalloidin (Thermo Fisher Scientific, 1:15 000 dilution) binding to the F-actin detects the plasma membrane. The membrane from the trans-well was stripped off using a blade and mounted with Fluoroshield mounting medium (Sigma-Aldrich, containing DAPI) on a glass coverslip. All images were acquired as mentioned previously.

Tyrosinase assay

For the tyrosinase assay, 1 × 10^5 YS cells were plated on each well of a six-well plate and kept overnight at 37°C and 5% CO_2. Post transfection the cells are washed twice using 1X PBS followed by the addition of acetone-methanol (1:1) for 30 s while being incubated on ice. This was followed by the addition of 1 ml of

L-DOPA (3,4-Dihydroxy-L-phenylalanine, Sigma-Aldrich) solution (0.15% W/V ratio in PBS) to each well and incubated at 37°C for 2 h. After 2 h cells were washed with PBS and imaged using an Inverted Microscope (Carl Zeiss™ PrimoVert™, ZEISS) under 40× magnification.

For quantification of the Dopachrome pigment intensity, images were converted to red, green, blue (RGB) format using Image J. The resolution and pixel intensity are adjusted as described.[6] Images are provided uniform background intensity by using the "threshold" option under "adjust" in the "image" tab. The pigment intensity and area are recorded and pigment intensity per unit area is represented.

Estimation of vesicle number and measurement of Pearson's correlation coefficient

The vesicle estimation in the confocal images of C6 cells has been performed using Image J Fiji software., At the beginning of image analysis, the scale of each image is set to μm. The image is then split into three channels (red, green, and blue) depending on the number of the fluorophore used during immunostaining. Only the channel for GFP tagged ATP 7B has been used for further analysis. The auto threshold of the image was then adjusted by choosing the "Otsu" option that represents the best background minimization. The region of interest (ROI), in the image, is appropriately selected to include only the regions (in the neurite and soma) where vesicles are present. This is done using the free hand tool. The numbers of vesicles in the selected ROI were then recorded by selecting the "analyse particles" option under "analyse" option. The total area (μm^2) is recorded by selecting the "measure" option under "analyse." The data are recorded and used to calculate the vesicles/μm^2. This whole process was repeated for analysing the neurite and the soma separately of each differentiated and undifferentiated C6 cell.

For measuring the Pearson's correlation coefficient (PCC), each of the confocal images was opened in Fiji (Image J). PCC has been performed by using the Coloc 2 program as already reported.[6]

Statistical analysis

The data were presented as mean values ± standard deviation. The GraphPad Prism 6 software compares differences between two groups using the Student's paired *t*-test (GraphPad Prism Inc., San Diego, CA, USA). The following standards are used to denote statistically significant differences between them: $^{*}P < 0.05$, $^{**}P < 0.01$, $^{***}P < 0.001$, and $^{****}P < 0.0001$.

Results

WD-causing ATP7B mutations exhibit variable stability

The effect of six WD-causing mutations on the intracellular stability of ATP7B was investigated. GFP-ATP7B (either WT or mutant) was transiently transfected into the HEK293T cells. The analysed mutations include N41S, S653Y, R778Q, G1061E, H1069Q, and T1434M (Supplementary Fig. S1). Absence of band for GFP-ATP7B in the UT confirms the signal from the transient expression (Fig. 1A, B) and not from the endogenous protein. Intense band in the WT lane shows optimum expression of the GFP-ATP7B (Fig. 1A, B) in the HEK293T cells. The WD mutations are observed to affect the stability of the GFP-ATP7B to varying degree. ATP7B-N41S (N41S mutant) exhibits minimum stability. The N41S mutant has only 1.6% stability compared to the WT ATP7B (Fig. 1C; Table 1). S653Y mutation causes 36.8% decrease in the stability of the ATP7B. ATP7B, harboring the R778Q has 31% stability compared to the WT counterpart (Fig. 1C; Table 1). G1061E bearing ATP7B is the second most common mutation among the Indian WD patients having a prevalence of 11% among the Indian population.[9] The G1061E mutant demonstrates 20.6% protein stability compared to the WT protein (Fig. 1C; Table 1). As it has been previously reported,[10] it has a lesser stability with respect to the WT ATP7B. ATP7B–H1069Q shows 42.2% protein stability, that corroborates with previous report.[8] ATP7B-T1434M has shown the highest stability among all the mutants, and it is comparable to the WT (Fig. 1C; Table 1) protein. Next, we investigated whether stability could dictate the intracellular localization of the GFP-ATP7B harboring the different WD mutations.

ATP7B mutants exhibit distinct intracellular localization in the HEK293T cells, which correlates with their stability

The intracellular localization of the GFP-ATP7B harboring the WD mutations are investigated in the HEK293T cells following transient transfection. The reduced stability of the N41S mutant interfered with the localization study due to extremely reduced signal intensity owing to the low protein level in the cells. Effects of S653Y[11] and H1069Q[8] on intracellular localization has been previously demonstrated. The effects of R778Q, G1061E and T1434M mutations were selected for further investigation. Under basal condition, ATP7B- R778Q (R778Q mutant) having less than 50% stability (Fig. 1C), compared to the WT, shows dual localization. A portion of the mutant protein co-localized with the TGN marker Golgin 97 (Fig. 2B). But a considerable fraction of the mutant protein does not localize on the TGN (Fig. 2B). Since the mutation considerably affects the protein stability, we investigated if the portion of the R778Q mutant, not in the TGN, localized into the endoplasmic reticulum (ER). The R778Q mutant demonstrates co-localization with the ER marker Calnexin (Supplementary Fig. S3). The dual localization, in the TGN and ER, was quantitated by calculating the PCC between ATP7B and the corresponding markers, Golgin97 and Calnexin (Supplementary Fig. S3). ATP7B-R778Q demonstrated higher PCC with the TGN marker (0.63) than Calnexin (0.36) (Supplementary Fig. S3B).

ATP7B-G1061E (G1061E mutant) also shows dual localization in the TGN and ER (Fig. 2C and Supplementary Fig. S3). This corroborates with its intracellular stability. G1061E mutant is less stable as compared to the R778Q mutation. Also, the PCC quantitation shows a higher co-localization of the G1061E mutant with Calnexin (0.53) than TGN (0.23) (Supplementary Fig. S3B) suggesting that the mutant protein localizes more on the ER than the TGN.

We wanted to investigate the ability of the mutants to traffic into vesicles in response to $CuCl_2$ treatment. The G1061E mutant was excluded as the majority of the mutant ATP7B localizes into the ER. The portion of the TGN localized R778Q mutant traffics into the vesicles in response to the treatment with 50 μM $CuCl_2$ (Fig. 2B, middle). This is evident from the loss of TGN localization of the mutant in response to $CuCl_2$ treatment (Fig. 2B, middle). The mutant can perform retrograde trafficking back to the TGN when treated with 50 μM $CuCl_2$ followed by 30 μM TTM (Fig. 2B, panel 3) as indicated by the localization of the protein on the TGN.

As observed in the case of previously demonstrated mutants, intracellular stability of ATP7B-T1434M (T1434M mutant) also corroborates nicely with its localization. The T1434M mutant, having comparable stability with the WT counterpart (Fig. 1C), shows localization at the TGN (Fig. 2D, upper panel). Next, we wanted to investigate its ability to traffic from the TGN to vesicles in

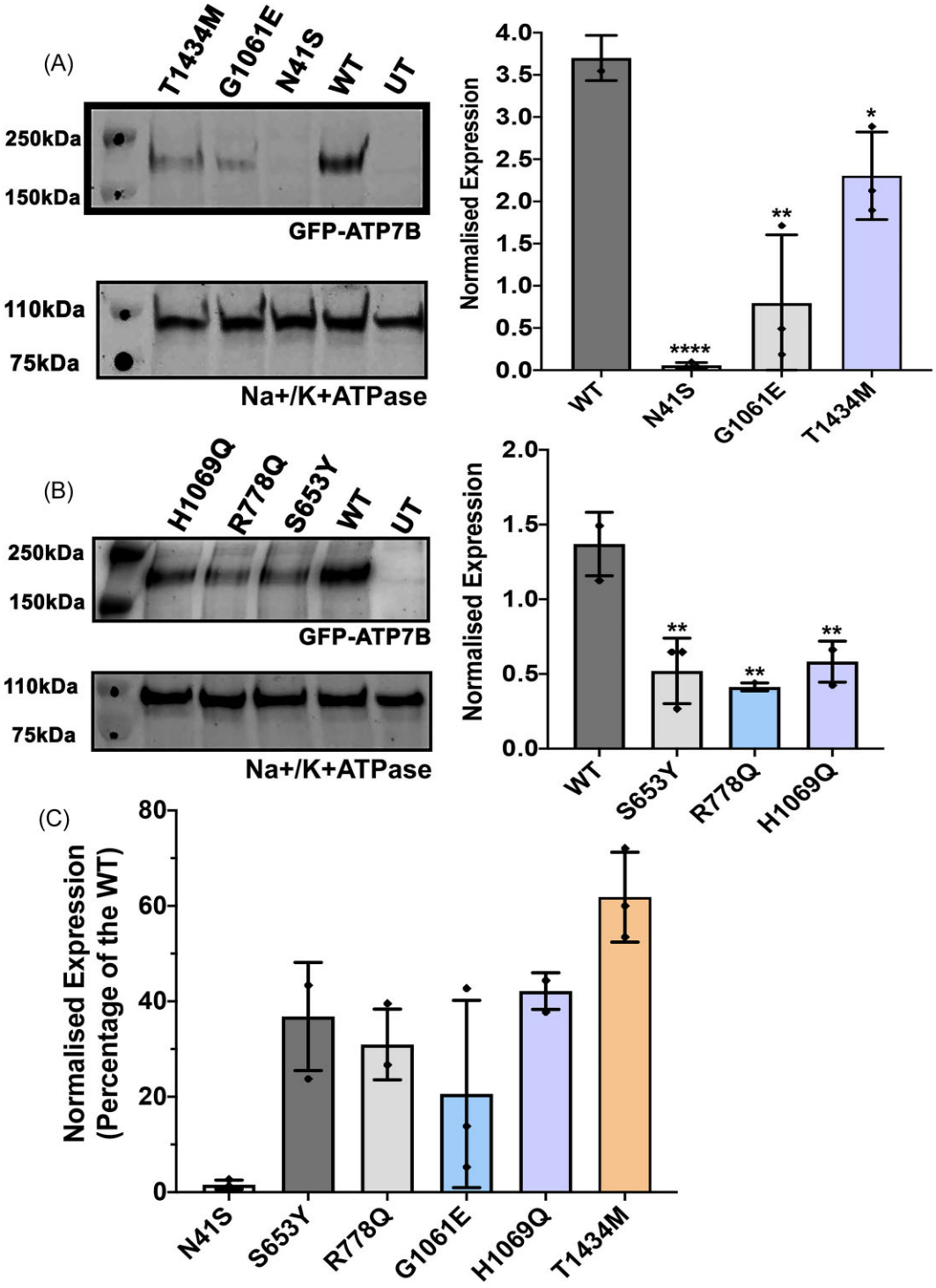

Fig. 1 Intracellular Stability of the GFP-ATP7B harboring the WD mutations. Panel A and B (Left side)—Western immunoblot showing WT ATP7B, and that harboring the WD mutations (upper—N41S, G1061E, T1434M, and lower—S653Y, R778Q, H1069Q). Absence of band for the GFP signal in the UT (un-transfected lane) confirms the transient expression of ATP7B. Panel A and B (right side)—Expression of the GFP-ATP7B (WT and the mutants) normalized to that of Na^+/K^+ ATPase calculated from the respective densitometries has been represented [(number of experimental replicates—3. Upper panel—****P-value < 0.0001, **P-value—0.0041, *P-value—0.0144. Lower panel **P-value—0.0086 (S653Y), **P-value—0.0015 (R778Q), **P-value—0.0057 (H1069Q)]. Panel C—Normalized expression of mutant GFP-ATP7B expressed as percentage to that of the WT counterpart. ATP7B-N41S—1.6%, ATP7B-S653Y—36.8%, ATP7B-R778Q—31%, ATP7B-G1061E—20.6%, ATP7B-H1069Q—42.2, ATP7B-T1434M—61.8%.

response to copper ($CuCl_2$) treatment. Interestingly, treatment with 50 μM $CuCl_2$ was unable to localize the T1434M mutant into the vesicles (data not shown) in contrast to the WT (Fig. 2A, panel 2). To further investigate, we studied the ability of the T1434M mutant to traffic in response to the treatment with a higher (100 μM) dose of $CuCl_2$ (Fig. 2D, lower panel). WT ATP7B localizes into the vesicles and even to the plasma membrane (Fig. 2A, panel 3) in response to the treatment with 100 μM $CuCl_2$. In contrast, the T1434M mutant localized mostly into the TGN (Fig. 2D, lower panel). This observation is further confirmed by investigating

Table 1. Various aspects of cellular copper homeostasis by ATP7B harbouring the WD-causing mutation

Mutations	Location (Exon)	Stability (% of WT)	Tyrosinase activity assay	Localization		Copper regulated trafficking		Comments and references
				ER	TGN	Anterograde	Retrograde	
N41S	before the first Cu binding domain of helix one, near to the N-terminal domain (2)	1.6[a]	No[a]	[c]	[c]	[c]	[c]	Present study
S653Y	between Cu binding domain 6 and first transmembrane helix (TM1) (7)	36.8[a]	Yes[b]	−[b]	++[b]	−[b] (WIF-B)		Present study and reported[11]
R778Q	fourth transmembrane helix (TM4) (8)	31[a]	Yes[a]	+[a]	++[a]	Partial[a] (HEK293T)	Partial[a]	Present study
G1061E	ATP binding domain (14)	20.6[a]	No[a]	++[a]	+[a]	−[b] (HEK293T)		Present study and reported[10]
H1069Q	ATP binding domain (14)	42.2[a]	Yes[a]	+[b]	+[b]	−[b] (Polarized MDCK)		Reported.[8]
S1423N	C-terminal domain (21)	Stable[b]	Yes[b]	−[a]	++[a] TGN (Differentiated C6 Only)	+[a] (Differentiated C6[a] , Polarized MDCK[b])	Partial[a] (Differentiated C6[a])	Present Study and reported[7]
S1426I	C-terminal domain (21)	Stable[b]	Yes[b]	−[a]	++ [a]	+[a] (Differentiated C6[a] ,HEK293[b])	+[a] (Differentiated C6[a])	Present study and reported[7,10]
T1434M	C-terminal domain (21)	61.8[a]	Yes[a]	−[a]	++[a]	+[a] (Differentiated C6[a] , Polarized MDCK[a] , WIF-B[b])	+[a] (Differentiated C6[a] ,WIF-B[b])	Present study and reported[15]

[a]Conclusion based on present study.
[b]Conclusion based on reference presented in the comments section
[c]Cannot be investigated due to the severe effect of the mutation on protein stability.
+/++: Extent of co-localization. −:Not present/unable to perform.

and comparing the co-localization of WT ATP7B and the T1434M mutant with the plasma membrane protein Na^+/K^+ATPase (Fig. 3). While the WT ATP7B localized into the vesicles and even co-localized with Na^+/K^+ATPase (Fig. 3, upper panel), the T1434M mutant neither localizes into vesicles nor co-localizes with Na^+/K^+ATPase (Fig. 3, lower panel) in response to 100 μM $CuCl_2$ treatment.

Intracellular localization of the ATP7B mutants revealed either dual localization at the ER and TGN (R778Q and G1061E mutants) or exclusively in the TGN (T1434M mutant). The intracellular localization of the mutants is largely dictated by their intracellular stability (Table 1). It would be interesting to investigate if the portion of TGN localized ATP7B harboring either R778Q or G1061E is able to perform copper [Cu(I)] transport activity under basal condition. Also, it is important to investigate if the T1434M mutant showing WT-like TGN localization can transport Cu(I) into the TGN lumen. Hence, we investigated the ability of the mutant ATP7B, localized into the TGN, to transport Cu(I) into the TGN lumen.

TGN localized ATP7B mutants exhibit copper [Cu(I)] transport capacity into the biosynthetic pathway

The Cu(I) transport ability of ATP7B, harboring the WD mutations, is investigated by testing its ability to transport Cu(I) into the TGN lumen. The transported Cu(I) is incorporated into tyrosinase and the terminal step of conversion of the L-DOPA to dopachrome within the TGN lumen[12] is visualized under phase contrast microscope. The assay is performed by co-transfecting Menkes Fibroblast cells, lacking any Cu-ATPases, with ATP7B (WT/mutant) and tyrosinase expression plasmids. The N41S mutant, having considerably reduced stability, failed to perform Cu(I) transport into the TGN (data not shown). We observed that the YS cells transiently expressing the R778Q mutant, could produce the dopachrome (Fig. 4). This demonstrates that the R778Q mutant, localizing mostly into the TGN can perform Cu(I) transport into the TGN lumen and shows dopachrome formation. The H1069Q mutant is able to produce dopachrome as reported[7] (Fig. 4). Whereas YS cells transiently expressing the G1061E mutant does not show formation of the dopachrome (Fig. 4). This demonstrates that the G1061E mutant, having considerably lower stability than the WT and localizing mostly into the ER fails to perform Cu(I) transport into the TGN. The T1434M mutant, having comparable stability to the WT and localizing to the TGN, can perform Cu(I) transport as revealed by the presence of dopachrome pigment in YS cells transiently expressing the mutant (Fig. 4). The results have been summarized in Table 1. Quantitation of the in-cell pigment generation did not show any significant difference between the mutants and the WT protein (Fig. 4B). However, the mutants might have differences in their Cu(I) transport capacity compared to their WT counterpart. But all the mutants can efficiently perform Cu(I) transport *in vivo*.

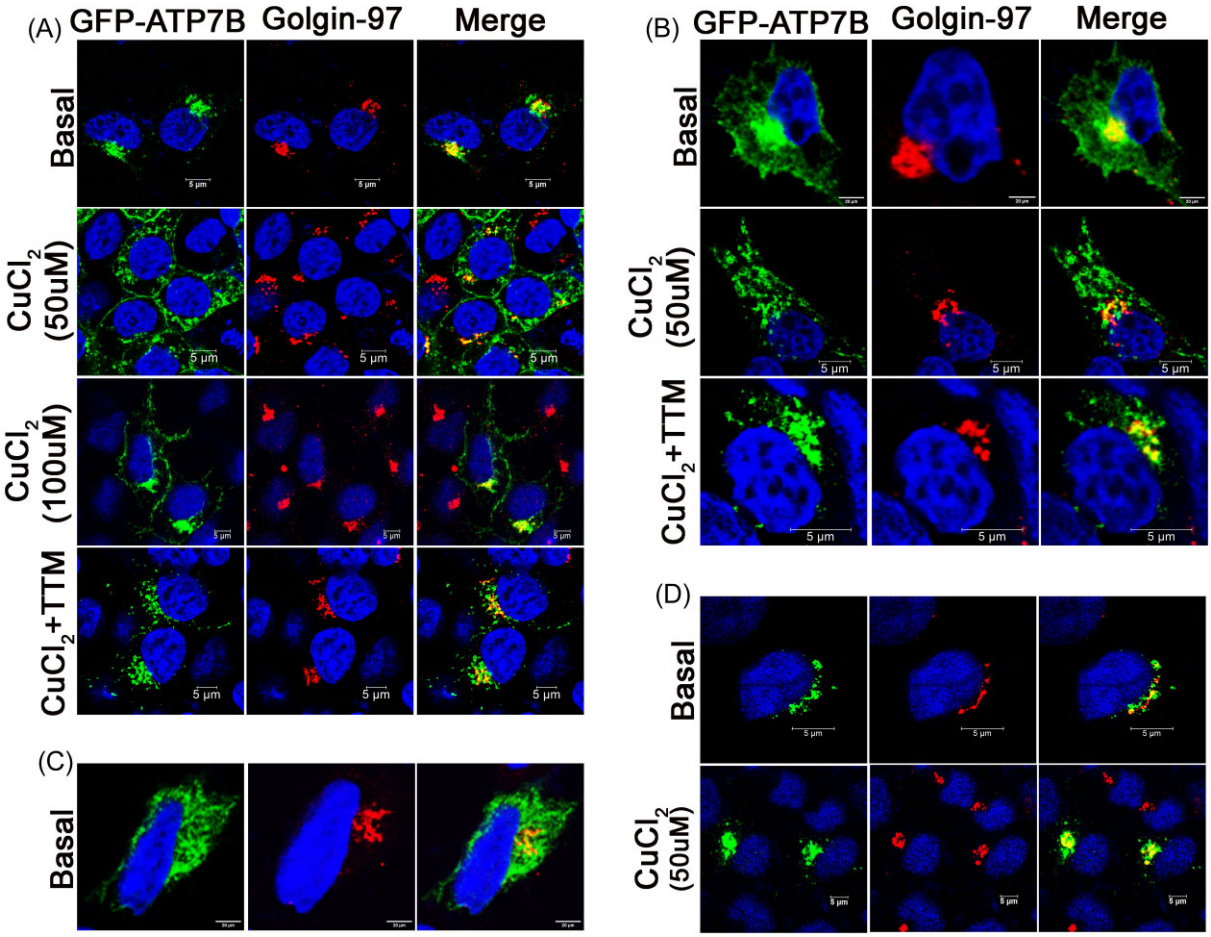

Fig. 2 Localization, anterograde, and retrograde trafficking of GFP-ATP7B harboring the R778Q, G1061E, and T1434M mutations in the HEK293T cells. A—WT ATP7B co-localizes with Golgin97 under basal condition (panel 1). WT ATP7B traffics to vesicles in response to 50 μM $CuCl_2$ (panel 2) and even to the plasma membrane (panel 3) in response to 100 μM $CuCl_2$. WT ATP7B traffics back to the TGN from vesicles in response to the treatment with 50 μM $CuCl_2$ followed by 30 μM TTM (panel 4). B—ATP7B-R778Q partially localized on the TGN under basal condition (panel 1). The TGN resident mutant protein traffics to the vesicles in response to 50 μM $CuCl_2$ treatment (panel 2). ATP7B-R778Q mutant can perform retrograde trafficking back to TGN in response to treatment with 50 μM $CuCl_2$ followed by 30 μM TTM (panel 3). C—ATP7B-G1061E localizes partially on TGN and other compartments under basal condition. D—ATP7B-T1434M localizes on the TGN like the WT ATP7B (upper panel) under basal condition. However, the T1434M mutant is unable to localize to vesicles even in response to 100 μM $CuCl_2$ treatment (lower panel). R778Q and G1061E mutants under basal condition—Images are captured with 100× oil immersion lens. Scale bar 20 μm. WT, R778Q mutant ($CuCl_2$ and $CuCl_2$ followed by TTM) and T1434M mutants—Images are captured at 63× oil immersion lens. Scale bar 5 μm.

ATP7B-T1434M can perform copper induced trafficking in the differentiated glia unlike that in the HEK293T cells

As already shown in the previous sections, ATP7B harboring the T1434M mutation showed comparable intracellular stability and localization like the WT counterpart. But the T1434M mutant does not exit TGN and vesicularize in the HEK293T cells in response to copper ($CuCl_2$) treatment. However, HEK293T cells are unpolarized non neuronal cells. WD patients exhibit both hepatic and neuronal symptoms[1,13,14] and both the organs comprise polarized cells, having unique proteome compared to the unpolarized cells. Further, the mechanism of WD mutations affecting neuronal copper homeostasis has not been investigated. Therefore, we wanted to investigate the ability of the T1434M mutant to perform the copper-dictated TGN exit and vesicular localization in the differentiated (C-6 derived) glial cells as a preliminary step to understand the mechanism of neuronal pathology associated with WD.

C-6 cells have been differentiated as already reported.[6] Undifferentiated and differentiated (glia) C-6 cells are transiently transfected with either WT or mutant (harboring T1434M) ATP7B. The T1434M mutant showed similar localization in the TGN (Fig. 5B, upper panel) as the WT protein (Fig. 5A, upper panel) in the undifferentiated C-6 cells. The WT ATP7B localized nicely into the intracellular vesicles in response to the treatment with 50 μM $CuCl_2$ (Fig. 5A, lower panel). Under such a condition, the T1434M mutant is arrested entirely in the TGN (Fig. 5B, lower panel) and does not localize to the vesicles like that observed in the HEK293T cells.

In the differentiated C-6 derived glia, under basal condition, WT ATP7B localized to the TGN and intracellular vesicles in the neurites (Fig. 6A, upper panel). Such vesicular localization, under basal condition, has been earlier observed for ATP7A in the glia.[6] Endogenous ATP7A localizes to RAB11 positive vesicles, in addition to the TGN, in the glia under basal condition.[6] Although the identity of the ATP7B containing vesicles has not been investigated in this case, yet it is suggestive that ATP7B shows similar localization in the glia, under basal conditions. The T1434M mutant localizes into TGN and intracellular vesicles in the glia (Fig. 6B, upper panel), like the WT protein under basal condition. Interestingly, the T1434M mutant can exit TGN and localize

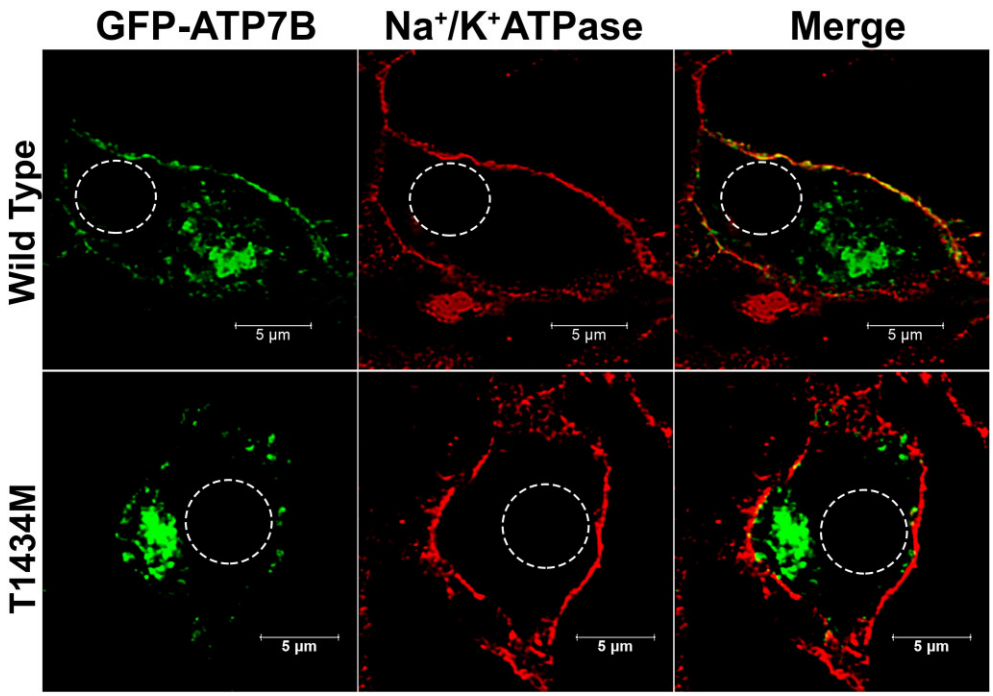

Fig. 3 Investigating the co-localization of GFP-ATP7B-T1434M with the Na^+/K^+ATPase in the HEK293T cells in response to the treatment with 100 μM $CuCl_2$. WT ATP7B vesicularizes and even localizes to the plasma membrane as demonstrated by the co-localization with Na^+/K^+ATPase. But ATP7B-T1434M is retained in the TGN and is not vesicularized. The nucleus has been demarcated with a dotted outline. Images are captured by 63× oil immersion lens. Scale bar 5 μm.

to the vesicles in response to 50 μM $CuCl_2$ (Fig. 6B, middle) like the WT protein (Fig. 6A, middle). The TGN exit of the mutant protein is evident from the increase in the number of vesicles both in the perinuclear region and the neurites (Fig. 6B, inset). This observation contrasts with what is observed in the HEK293T and undifferentiated C-6 cells. To further confirm the copper-dictated trafficking of ATP7B in the glia, we quantitated the total number of vesicles per area (per square micrometer). As expected, statistically significant increase in the number of vesicles per square micrometer (μm^2) is observed both in the soma and neurites of the glia transiently expressing the WT ATP7B (Supplementary Fig. S4A) in response to $CuCl_2$. We observed similar increase in the number vesicles in the glia transiently expressing the T1434M mutant (Supplementary Fig. S4B). The number of vesicles per area increased both in the soma and neurite region of the glia (Supplementary Fig. S4B) in response to copper treatment. Together the results demonstrate that the T1434M mutant is unable to perform copper-dictated vesicular trafficking in the HEK293T cells and undifferentiated C-6 cells. However, the mutant ATP7B can perform copper-dictated vesicular localization in the differentiated glia. Not only anterograde trafficking, ATP7B-T1434M can perform retrograde trafficking back to the TGN (Fig. 6B, lower panel), like the WT ATP7B (Fig. 6A, lower panel), in response to the treatment with 50 μM $CuCl_2$ followed by the treatment with 50 μM TTM. However, a slightly higher concentration of TTM (50 μM instead of 30 μM as in previous case) is needed to bring back most of the WT and mutant protein to the TGN in the differentiated C-6 glia.

Next, we wanted to investigate whether both the WT and T1434M mutant localized to similar vesicles in response to $CuCl_2$ treatment. C-6 cells are co-transfected with GFP-ATP7B-T1434M and mKO2-wtATP7B followed by differentiation into glia and treatment with 50 μM $CuCl_2$. Both WT and T1434M mutant localized to the same vesicles in response to $CuCl_2$ treatment (Fig. 6C) suggesting that the Cu(I) responsive trafficking property of T1434M mutant is like the WT ATP7B in the glia.

C-6 cells express ATP7A and do not express ATP7B.[6] Nevertheless, the two copper transporters should be able to perform copper-dictated TGN exit as they have similar trafficking route in the unpolarized cells. But since C-6 cells do not express ATP7B, the differentiated (C-6 derived) glia might not express the unique trafficking partners required for the polarized apical trafficking of ATP7B. Despite this issue, we observed copper-dictated vesicularization of ATP7B in the glia. Nevertheless, to further confirm our observation, we investigated copper-dictated trafficking property of the T1434M mutant in another polarized system. We investigated the ability of the T1434M mutant to localize into the vesicles in the polarized MDCK cells, which has been demonstrated to express ATP7B and has been utilized to study the polarized trafficking of the ATP7B harboring WD mutations.[7]

ATP7B-T1434M can perform copper induced trafficking into the vesicles in the polarized MDCK cells like that in the glia

MDCK cells are polarized as reported.[7] Polarization is confirmed by the expression of podocalyxin (Gp135) on the apical and sodium potassium ATPase on the basolateral plasma membrane (Supplementary. Fig. S5). In the unpolarized MDCK cells, the T1434M mutant (Fig. 7B, upper panel) showed localization into the TGN like the WT ATP7B (Fig. 7A, upper panel). The mutant protein is unable to exit TGN in response to 50 μM $CuCl_2$ (Fig. 7B, lower panel), like the HEK293T and the undifferentiated C-6 cells. In the polarized MDCK cells, under basal condition, the T1434M mutant (Fig. 8B, upper panel) is localized like WT ATP7B (Fig. 8A, upper panel) into the TGN. However, it can exit TGN and localize to vesicles in the polarized MDCK cells (Fig. 8B, lower panel)

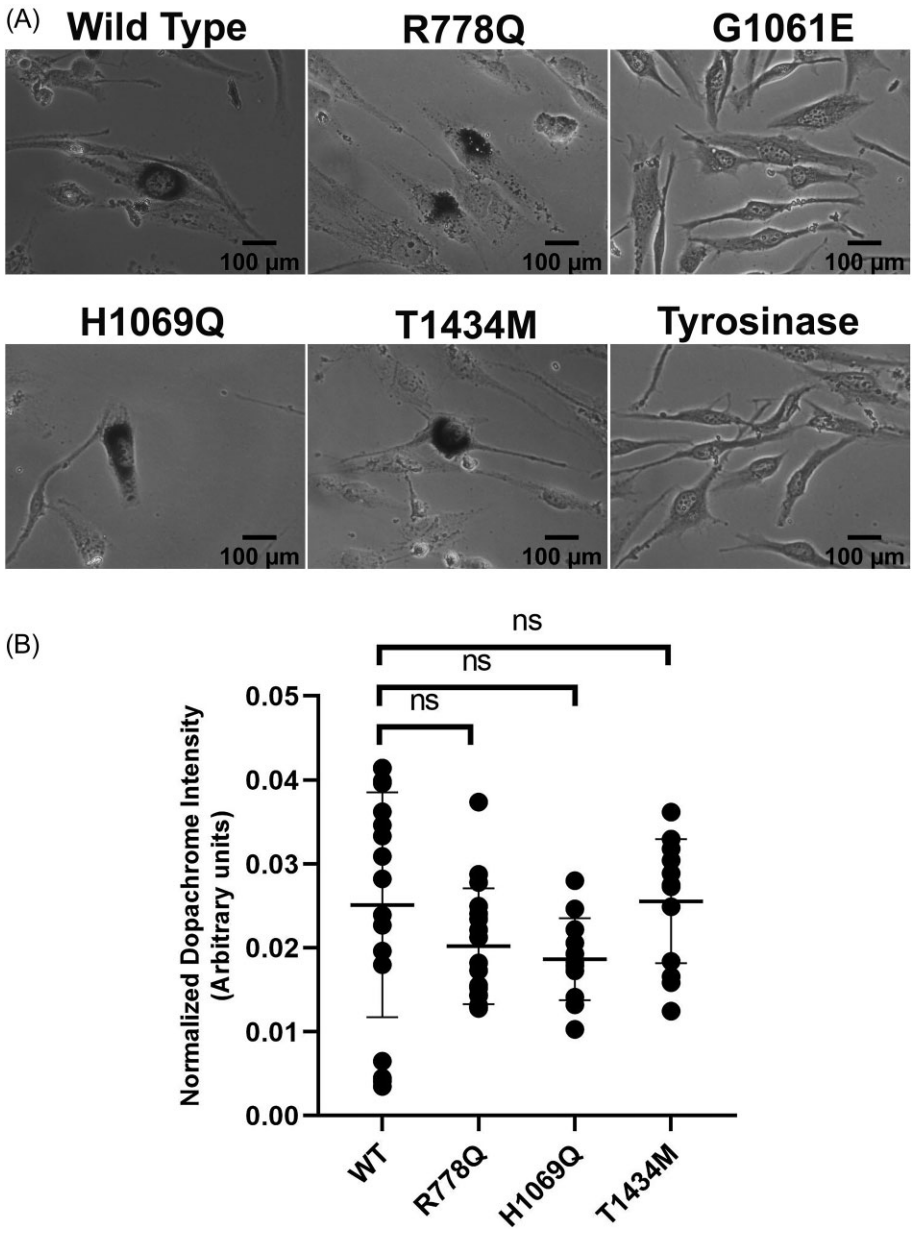

Fig. 4 Copper [Cu(I)] transport activity into the lumen of the TGN by GFP-ATP7B harboring the WD mutations. A—WT ATP7B, ATP7B-R778Q, ATP7B-H1069, and ATP7B-T1434M can export Cu(I) into the TGN as is demonstrated by the presence of the black Dopachrome pigment. However, ATP7B-G1061E cannot perform this function as demonstrated by the absence of Dopachrome. Cells that are transfected with only the expression plasmid for tyrosinase do not form Dopachrome due to the presence of the nonfunctional ATP7A and absence of ATP7B in the Menkes disease fibroblast cells. Images were captured at 40× magnification. Scale bar 100 μm. B—Normalized quantitation of the Dopachrome pigment intensity has been represented. [$n = 18$ (WT), $n = 17$ (R778Q), $n = 12$ (H1069Q), $n = 13$ (T1434M).]

in response to 50 μM $CuCl_2$ treatment. The trend of the data is nicely reflected in the quantitation of the PCC for GFP-ATP7B and TGN marker (TGN38 in the glia and Golgin97 in the MDCK) in the undifferentiated (Fig. 9A) and differentiated C-6 (Fig. 9B), and unpolarized (Fig. 9C) and polarized (Fig. 9D) MDCK cells. WT ATP7B and TGN38 demonstrate a significant decrease (0.44 in presence of 50 μM $CuCl_2$ from 0.71 under basal condition) in the PCC in the undifferentiated C-6 cells (Fig. 9A) demonstrating the TGN exit of ATP7B. Under this condition there is no significant change in the PCC for the T1434M mutant and TGN38 (0.69 under basal condition and 0.66 in presence of 50 μM $CuCl_2$) in the undifferentiated C-6 cells (Fig. 9A) suggesting that the mutant does not exit TGN in these cells. But the mutant ATP7B and TGN38 shows a significant decrease in the PCC (0.38 in presence of 50 μM $CuCl_2$ from 0.54 under basal condition) in the differentiated (C-6) glia (Fig. 9B). Similarly, the T1434M mutant and Golgin97 show no significant change in the PCC (0.62 under basal condition and 0.6 in presence of 50 μM $CuCl_2$) value in the unpolarized MDCK cells (Fig. 9C). Like glia, the mutant protein shows a significant decrease in the PCC (0.43 in presence of 50 μM $CuCl_2$ from 0.59 under basal condition) for ATP7B and Golgin97 in response to $CuCl_2$ treatment demonstrating TGN exit (Fig. 9D). The results demonstrate that the T1434M mutant can traffic to the vesicles in the glia and polarized MDCK cells. The mutant has been reported to also traffic to vesicles in response to elevated Cu(I) in the WIF-B cells.[15] However, this copper-dictated trafficking of the T1434M mutant is

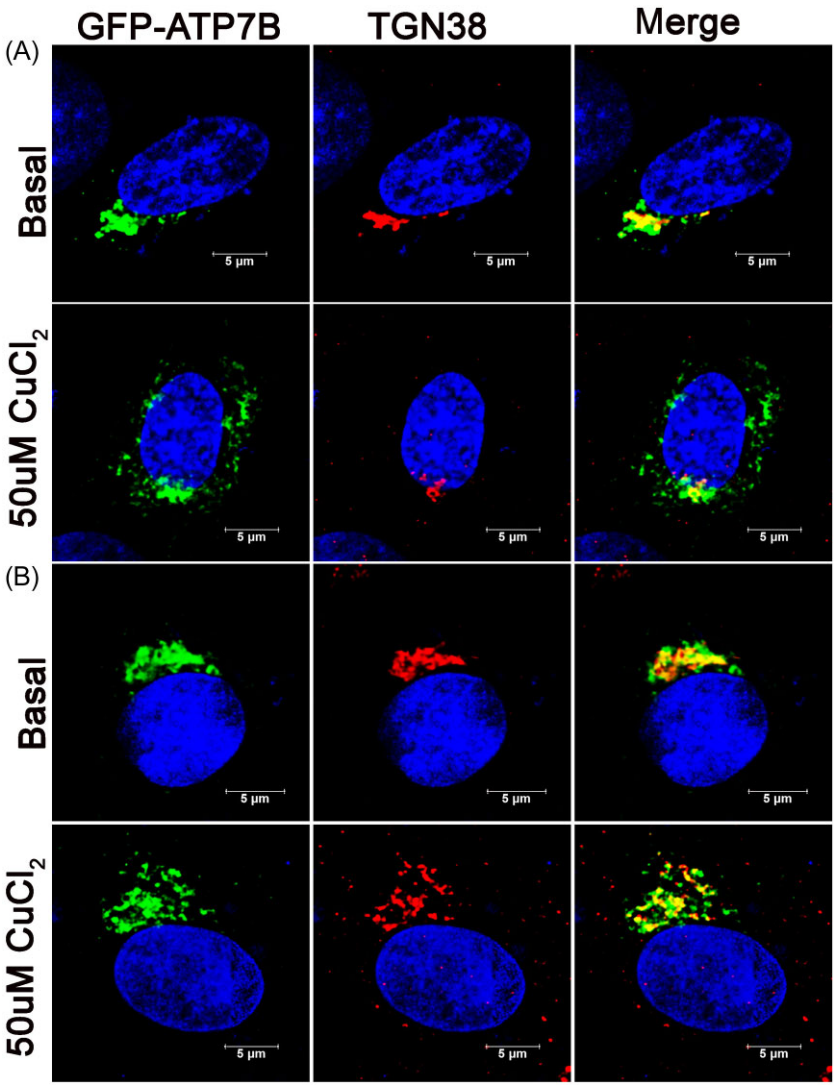

Fig. 5 Localization and Trafficking of GFP-ATP7B harboring the T1434M mutation in the undifferentiated C6 cells. A—WT ATP7B localizes into the TGN as demonstrated by its co-localization with TGN38 (upper panel). WT ATP7B localizes into intracellular vesicles, in addition to TGN, in response to the treatment with 50 μM $CuCl_2$ (lower panel). B—ATP7B-T1434M localizes on the TGN under basal condition (upper panel). This is demonstrated by its co-localization with TGN38. The mutant protein fails to exit the TGN and localize to the vesicles in response to the treatment with 50 μM $CuCl_2$ (lower panel). Images are captured by 63× oil immersion lens. Scale bar 5 μm.

not observed in the unpolarized MDCK, undifferentiated C-6, and HEK293T cells. This difference in the trafficking property is striking and has not been observed in case of any reported WD-causing mutations in ATP7B till date.

ATP7B-S1423N localizes to the TGN in the glia and not in the undifferentiated C-6 cells

The T1434 residue resides on the C-terminus of ATP7B. There is another reported WD mutation S1423N, which is situated few residues upstream to the 1434 residue in the C-terminus of ATP7B. The mutation involves a conservative substitution of amino acid with polar uncharged side chains. Although the intracellular localization of ATP7B harboring this mutation has already been studied,[7] we wanted to investigate whether the intracellular localization of this mutant shows any difference in the polarized vs. unpolarized cells. ATP7B-S1423N (S1423N mutant) does not co-localize with TGN38 in the undifferentiated C6 cells (Fig. 10A, upper panel) under basal condition. This is also demonstrated in the lower PCC value (0.08) of both the fluorophores (Fig. 10D). The mutant neither localizes on the TGN nor traffics into the vesicles in response to the treatment with 50 μM $CuCl_2$ (Fig. 10A, lower panel). But the mutant ATP7B shows a significant co-localization with TGN38 in the differentiated (C6) glia (Fig. 10B, upper panel) which is also evident from the significant increase in the PCC (0.37) of co-localization of the two fluorophores (Fig. 10D). It is probable that the extent of co-localization might not be comparable to the WT ATP7B. Nevertheless, the extent of TGN enrichment of the S1423N mutant is significant in the differentiated glia. Unlike the undifferentiated cells, S1423N mutant can traffic to the vesicles in response to the $CuCl_2$ treatment (Fig. 10B, middle panel) and traffic back to the TGN in response to $CuCl_2$ followed by TTM treatment (Fig. 10B, lower panel). However, the retrograde trafficking is partial as most of the mutant protein cannot traffic back to TGN (Fig. 10B, lower panel). The partial TGN retrieval of S1423N mutant has been confirmed at higher dose (70 μM) of TTM (Fig. 10B). Low PCC value (0.21) after TGN retrieval compared to the basal PCC value (0.37) confirms partial TGN retrieval of the

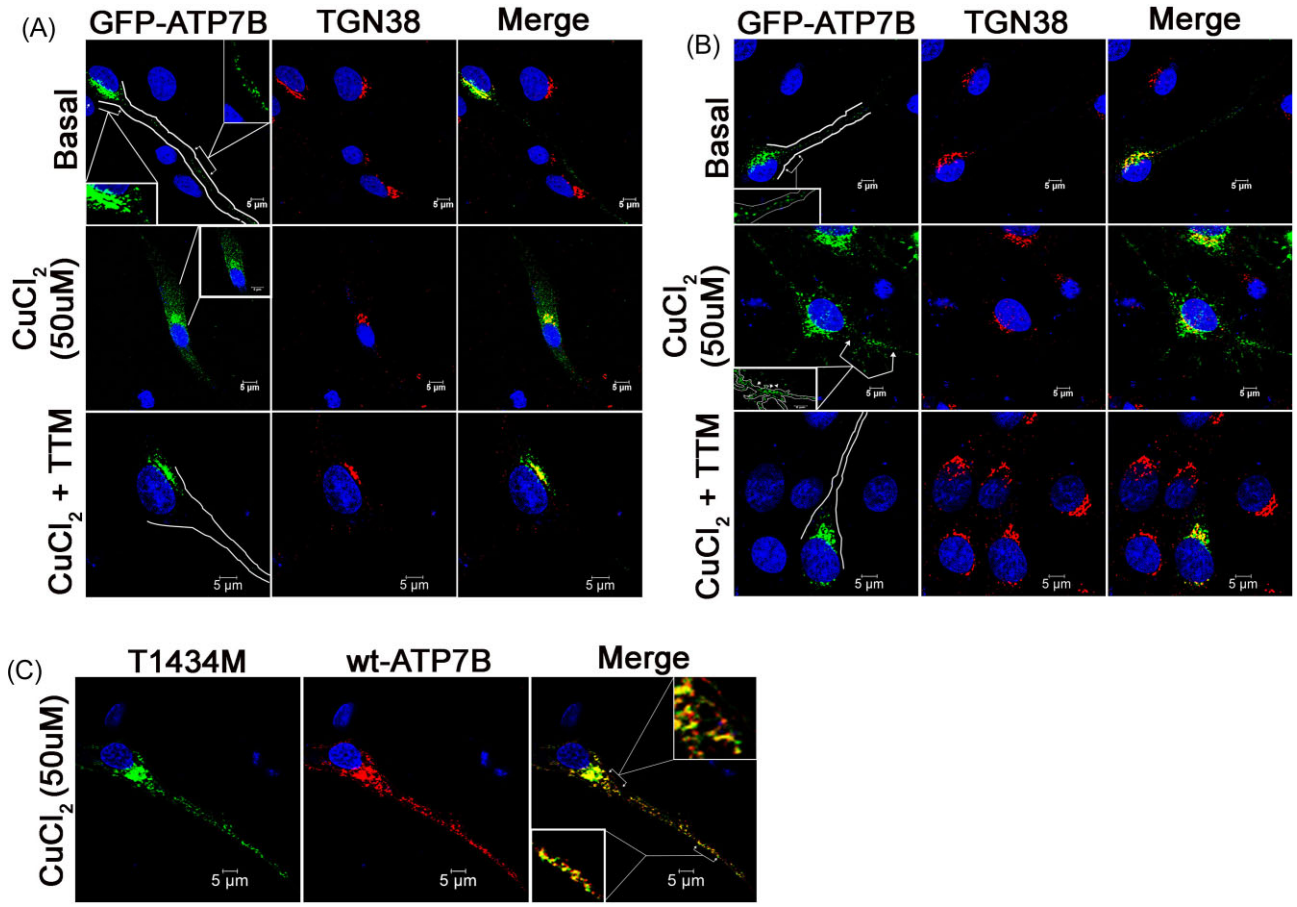

Fig. 6 Localization, anterograde, and retrograde trafficking of ATP7B-T1434M in the differentiated (C-6) glia. A—WT ATP7B localizes to the TGN as demonstrated by its co-localization with TGN38 (upper panel). In addition, ATP7B also localizes into vesicles along the neurite extensions (upper panel). Inset—portion of the soma and the neurite region has been magnified and demonstrated. WT ATP7B localizes to the intracellular vesicles near the soma in response to the treatment with 50 μM $CuCl_2$ (middle). Inset—A magnified region around the soma has been demonstrated. Wild-type ATP7B traffic from the vesicles back to the TGN in response to treatment with 50 μM $CuCl_2$ followed by treatment with 50 μM TTM (lower panel). B—ATP7B-T1434M localizes to the TGN as well as the vesicles along the neurite processes (upper). ATP7B-T1434M localizes on small intracellular vesicles both in the soma and along the neurites in response to the treatment with 50 μM $CuCl_2$ (middle). A region of the neurite has been magnified and represented in the inset. It demonstrates the ability of ATP7B-T1434M to exit the TGN in response to the $CuCl_2$ treatment. ATP7B-T1434M can traffic back to the TGN from vesicles in response to treatment with 50 μM $CuCl_2$ followed by treatment with 50 μM TTM (lower panel). C—Co-localization of GFP-ATP7B-T1434M and mKO2-wt-ATP7B in the differentiated C-6 cells. A region of the neurite has been magnified to show co-localization of the mutant and WT ATP7B.

mutant (Fig. 10D). We further investigated whether the mutant protein traffics to the same vesicles as the WT protein in response to high Cu(I). The majority of the mutant protein does not co-localize into the same vesicles as the WT ATP7B in response to $CuCl_2$ treatment (Fig. 10C).

Although the exact localization phenotypes are different for the S1423N and T1434M mutations in ATP7B, both the mutations show differences in the phenotypes in the polarized vs. unpolarized cells. While effects of the T1434M mutant are completely corrected in the polarized cells, S1423N shows partial correction. The localization of the S1423N mutant is corrected in the differentiated glia. But the anterograde and retrograde trafficking properties of the mutant is not completely identical to the WT protein. Future studies are necessary to investigate if Cu(I) responsive vesicular localization of S1423N can efficiently export Cu(I) from the cells. However, this suggests that the signal for these differences in the polarized and unpolarized cells primarily originates from the C-terminus of ATP7B. This further suggests presence of unique protein–ATP7B interactions in the polarized MDCK and the differentiated glial cells, which dictates ATP7B's localization and exit from the TGN. The data also suggest that these unique interactions might be mediated by the C-terminus of ATP7B.

ATP7B-S1426I mutant can traffic in response to $CuCl_2$ in the differentiated glia but not in the undifferentiated C-6 cells

To further confirm our hypothesis, we compared the localization, anterograde, and retrograde trafficking of ATP7B harboring the WD-causing mutation S1426I. Like T1434M mutant, the S1426I mutant localized on the TGN both in the undifferentiated (Fig. 11A, upper panel) and differentiated (Fig. 11B, upper panel) C-6 cells. Also, the mutant does not traffic to the vesicles in response to $CuCl_2$ in the undifferentiated C-6 cells (Fig. 11A, lower panel and C). But the mutant can traffic to vesicles in response to $CuCl_2$ in the differentiated (C-6) derived glia (Fig. 11B, middle panel and C). The mutant can also traffic back to the TGN in response to $CuCl_2$ followed by TTM treatment (Fig. 11B, lower panel). Also, the mutant traffics to the same vesicles as the WT ATP7B as

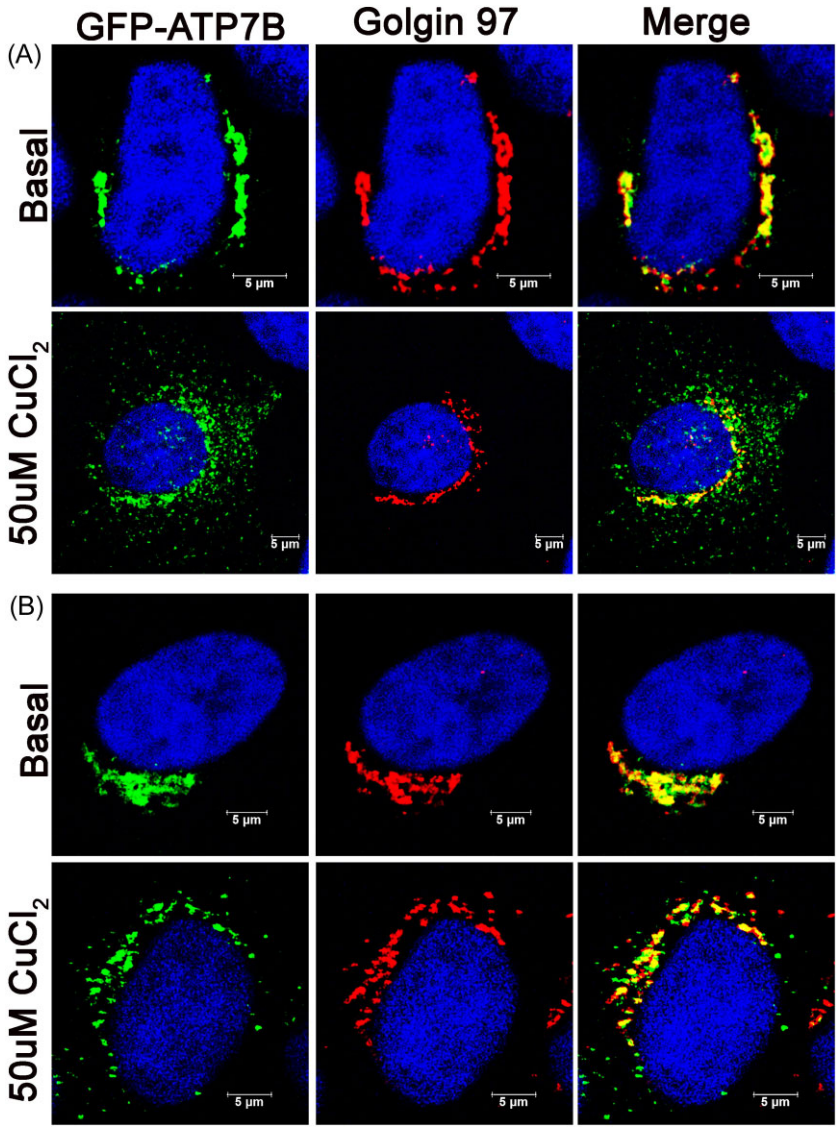

Fig. 7 Localization of WT ATP7B and ATP7B-T1434M in the unpolarized MDCK cells under basal and $CuCl_2$ treatment. Panel A (upper)—Under basal condition WT GFP-ATP7B co-localizes with Golgin97 demonstrating TGN localization. Lower panel—WT ATP7B localizes to intracellular vesicles in response to the treatment with 50 μM $CuCl_2$. Panel B (Upper)—ATP7B-T1434M localizes to the TGN, under basal condition, like the WT protein. Lower panel—ATP7B-T1434M fails to traffic to the vesicles and is retained in the TGN in response to the treatment with 50 μM $CuCl_2$. Images are captured by 63X oil immersion lens. Scale bar 5 μm.

demonstrated by the co-localization of the GFP-ATP7B-S1426I and mKO2-ATP7B (Fig. 11D).

WD mutations in the C-terminus of ATP7B show distinct cellular phenotypes

The effects of the individual mutations need to be investigated in relevant cell-based model to understand their contribution towards the nature and severity of the disease manifestation. C-terminus is the seat of WD mutations and effects of many of these mutations, on ATP7B stability and function have not been tested in relevant cell lines. We present a meta-analysis of the WD mutation in the C-terminus, effects of which have been investigated in the cell-based model. Such studies demonstrate that the C-terminus of ATP7B harbors WD mutations with distinct cellular phenotypes. Mutations situated in the proximal part of the C-terminus affect protein stability in the cells (Table 2). For example, substitution of Leu1373 residue with either arginine or proline affects the stability of ATP7B in the MDCK cells.[7] Studies done so far indicate that the missense mutations affecting residues Leu1373 to Gln1399 affect the stability of ATP7B (Table 2). This suggests that the proximal region of the C-terminus regulates the stability of ATP7B mainly by interdomain contacts. These mutations will therefore affect copper transport and export functions depending on their severity. WD mutations affecting Trp1410 onward do not affect the stability of the ATP7B within the cells. Among them, S1423N affects TGN localization in the undifferentiated cells, which is corrected in the differentiated glia. Anterograde and retrograde trafficking of the S1423N mutant is, however, affected in the differentiated glia as the mutant is unable to traffic to the same vesicles and retrieve back completely to the TGN like the wt-ATP7B. S1426I and T1434M mutations affect the TGN localization, only in the unpolarized cells, as indicated in the present study (Table 2). The effects of the mutations are completely corrected in the polarized cells. The brain, liver, and kidney, the main site of WD-mediated copper accumulation, are composed mainly

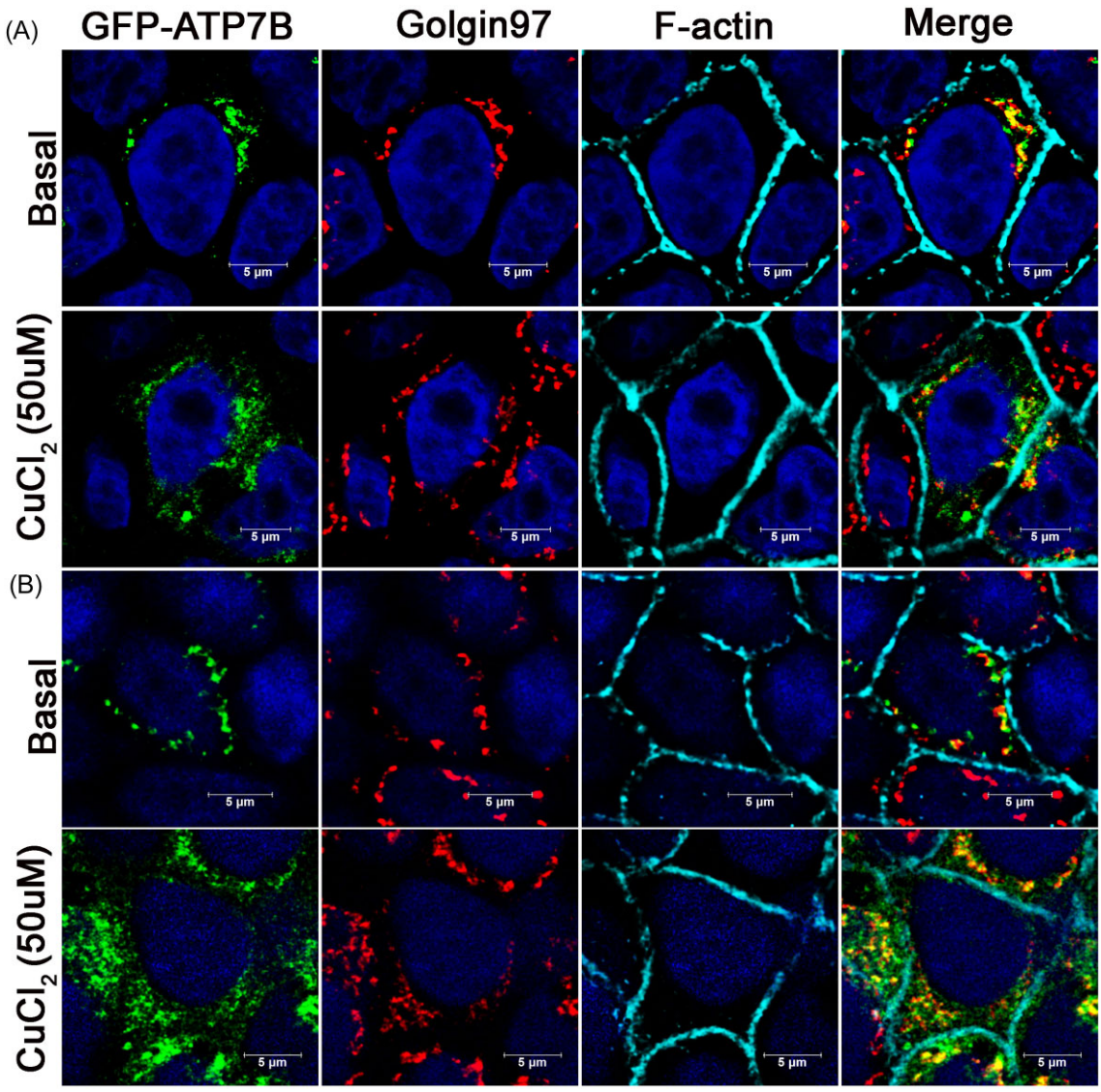

Fig. 8 Localization and Trafficking of ATP7B-T1434M in polarized MDCK cells. A—under basal condition WT ATP7B co-localizes with Golgin97 demonstrating TGN localization (upper panel). WT ATP7B localizes into the intracellular vesicles in response to the treatment with 50 μM $CuCl_2$ (lower panel). Cells have been probed with Alexa Fluor 647 phalloidin (cyan) binding to the F-actin to demonstrate the cell boundary. B—ATP7B-T1434M localizes into the TGN under basal condition (upper panel). The mutant protein localizes to the vesicles in response to the treatment with 50 μM $CuCl_2$ (lower panel). Images were captured at 63× oil immersion condition. Scale bar 5 μm.

of polarized cells. The effects of S1423N, T1434M, and S1426I on ATP7B are corrected in the polarized MDCK and differentiated glia indicating milder effects of these mutations in the organs composed of polarized cells. Genetic studies have reported these mutations only in the compound heterozygous form[16–18] indicating the requirement of a second debilitating mutation toward the disease pathogenesis.

Discussion

The various WD mutations included in this study have variable effects on the stability of ATP7B. N41S mutation, located on the N-terminus has the most drastic effect on the intracellular stability of ATP7B. This is followed by G1061E located on the ATP-binding domain and R778Q located on the transmembrane-4 (Fig. 1). However, the C-terminus mutations S1423N, S1426I, and T1434M have less or no effect on the stability of ATP7B. Further, the present study demonstrates the correlation between the intracellular stability and the localization of ATP7B harboring the WD mutations. Among the least stable WD mutants N41S and G1061E (Fig. 1), the G1061E mutant is localized primarily on the ER (Supplementary Fig. S3). The effect of R778Q is intermediate, and the mutant protein shows dual localization on the TGN and ER (Fig. 2, Supplementary Fig. S3). The TGN resident R778Q mutant protein can perform Cu(I) regulated anterograde and retrograde trafficking (Fig. 2). T1434M mutation does not affect the intracellular stability of ATP7B. The T1434M mutant has similar localization as the WT protein under basal condition (Fig. 2). The findings demonstrate that intracellular stability of the mutant ATP7B dictates its intracellular localization, which in turn dictates the ability of the mutant ATP7B to perform Cu(I) transport into the TGN (Fig. 4).

The T1434M mutant localizes on the TGN irrespective of the polarization of the cells. But the copper regulated trafficking of the T1434M mutant is dictated by the polarization of the cells. The T1434M mutant is unable to traffic to the vesicles under $CuCl_2$

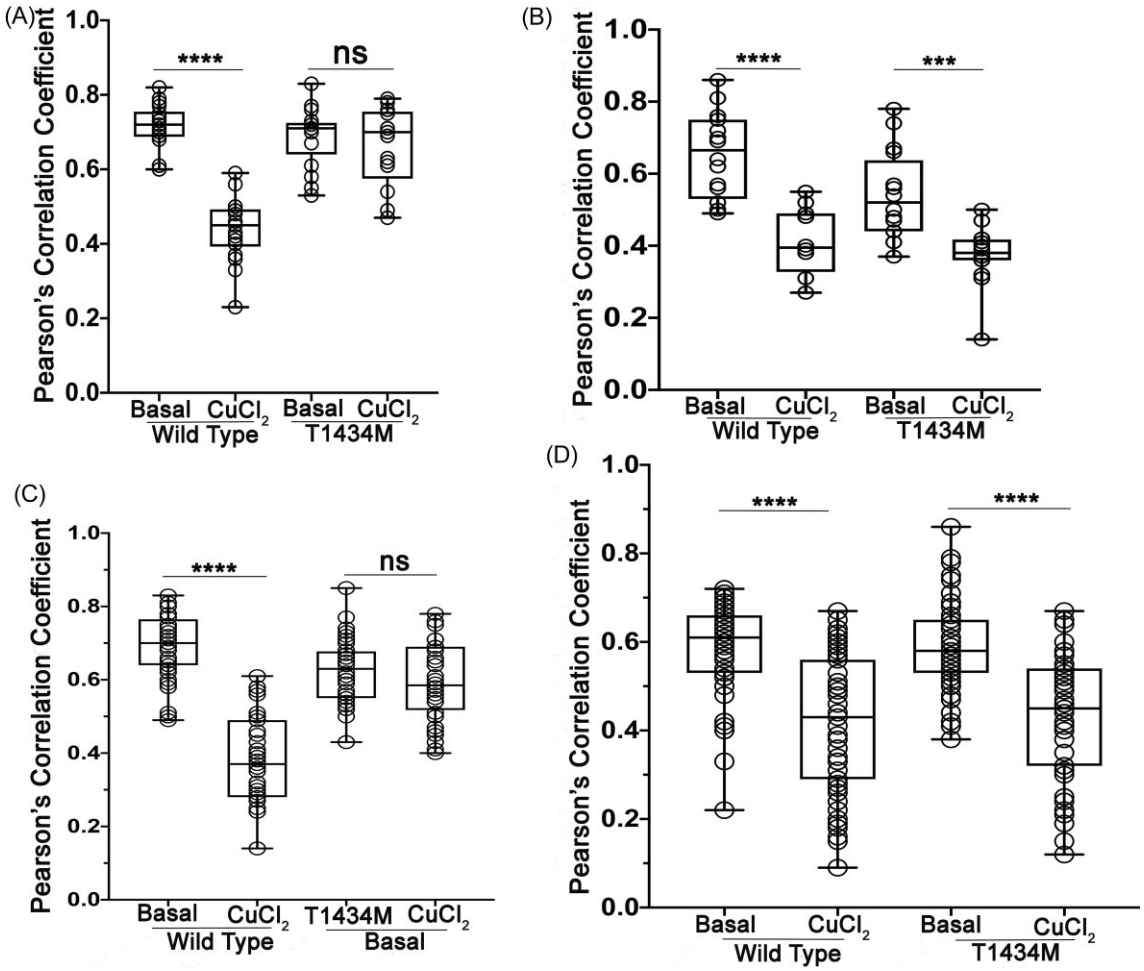

Fig. 9 Quantitative comparison of the co-localization of ATP7B-T1434M and the TGN markers in the undifferentiated/differentiated C-6 and unpolarized/polarized MDCK cells. Panel A—comparison of the co-localization of the WT/ATP7B-T1434M with TGN38 in the undifferentiated C-6 cells. The WT protein shows significant decrease in the PCC [0.44 in presence of $CuCl_2$ ($n = 18$) from 0.71 under basal condition ($n = 18$)] with TGN38 under $CuCl_2$ treatment. ****P-value < 0.0001. But ATP7B-T1434M and TGN38 shows no significant change in the PCC [0.69 under basal condition and 0.66 under $CuCl_2$ treatment ($n = 17$ under both conditions)] in response to $CuCl_2$ treatment. Panel B—comparison of the co-localization of the WT/ATP7B-T1434M with TGN38 in the differentiated (glia) C-6 cells. As in the undifferentiated cells, the WT protein shows significant decrease in the PCC [0.65 under basal condition and 0.42 under $CuCl_2$ treatment ($n = 16$ under both conditions)] with TGN38 in response to the $CuCl_2$ treatment. ****P-value < 0.0001. ATP7B-T1434M also shows significant decrease in the PCC [0.54 under basal and 0.38 under $CuCl_2$ treatment ($n = 16$ under both conditions)] with TGN38 under $CuCl_2$ treatment. ***P-value—0.0001. Panel C: Comparison of the PCC for WT/ATP7B-T1434M and Golgin97 in the unpolarized MDCK cells. The WT protein and Golgin97 shows significant decrease in the PCC [0.69 under basal condition ($n = 40$) and 0.38 under $CuCl_2$ treatment ($n = 39$)] in response to $CuCl_2$ treatment. ****P-value < 0.0001. But ATP7B-T1434M and TGN marker shows no change in the PCC [0.62 under basal condition and 0.6 under $CuCl_2$ treatment ($n = 40$ under both conditions)] in response to $CuCl_2$ treatment. Panel D: Comparison of the PCC for WT/ATP7B-T1434M with Golgin97 in the polarized MDCK cells. The WT protein and Golgin97 shows decreased PCC [0.58 under basal condition and 0.42 ($n = 55$ under both conditions)] under $CuCl_2$ treatment. Similarly, ATP7B-T1434M and Golgin97 also show decreased PCC [0.59 under basal condition and 0.43 under $CuCl_2$ treatment ($n = 55$ under both conditions)] in response to $CuCl_2$ treatment. ****P-value < 0.0001.

treatment in the HEK293T (Fig. 2), undifferentiated C-6 (Fig. 5), and unpolarized MDCK cells (Fig. 7). However, the mutant protein can traffic to vesicles in the differentiated glia (Fig. 6), polarized MDCK cells (Fig. 8), and WIF-B cells.[15] This selective trafficking of mutant ATP7B is unique and has not been demonstrated before. Not only that, T1434M mutant localizes to the same vesicles as the WT protein in response to $CuCl_2$ and can retrieve back to the TGN at low Cu(I). S1426I mutant behaves exactly like the T1434M mutant. Its trafficking (both anterograde and retrograde) behavior is corrected in the differentiated glia. Although not exactly similar, the S1423N mutant also shows localization dictated by the polarization of the cells. The S1423N mutant localizes into the TGN only in the differentiated glia under basal condition (Fig. 10). The S1423N mutant has been reported to localize on the TGN in the polarized MDCK[7] cells. But S1423N mutation prevents ATP7B from localizing on the TGN in the undifferentiated cells under basal condition (Fig. 10). However, the Cu(I) responsive vesicular localization of S1423N mutant is different from that of the WT protein. Consequently, the mutant cannot retrieve back to the TGN under low Cu(I). The identity of the vesicles, their Cu(I) export ability, and effect of partial TGN retrieval of the mutant are unclear and need to be studied. The mutant can localize into vesicles at high Cu(I) in the polarized MDCK cells but cannot localize to the apical plasma membrane[7] like the WT. The results demonstrate that the mutant can traffic in response to high Cu(I). But the Cu(I) regulated localization, in both glia and polarized MDCK, is not like the WT ATP7B. The cellular phenotypes demonstrated by the C-terminal mutants, despite being different, are rescued in the differentiated glia and polarized MDCK and manifested only in the unpolarized/undifferentiated cells. Further the results

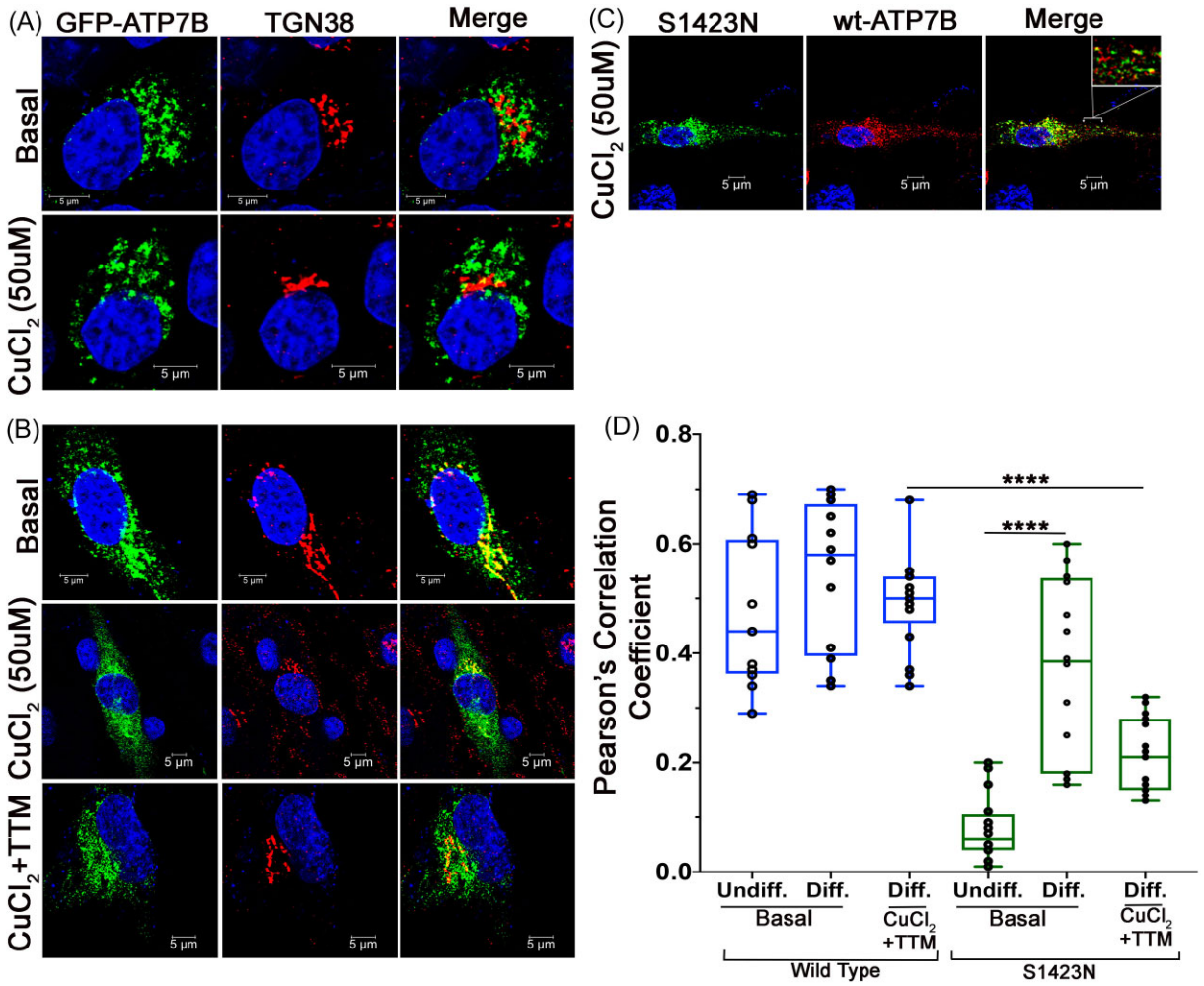

Fig. 10 Localization, anterograde and retrograde trafficking of GFP-ATP7B harboring the S1423N mutation in the undifferentiated and differentiated (glia) C-6 cells. A—The ATP7B-S1423N does not localize on the TGN under basal condition (upper panel) in the undifferentiated C-6 cells. The mutant protein does not traffic to the vesicles in the undifferentiated C-6 cells (lower panel). B—The mutant protein co-localizes considerably with TGN38 in the differentiated glia demonstrating localization into the TGN (upper panel). The mutant traffics to the vesicles in response to treatment with 50 μM $CuCl_2$ (middle). The mutant shows partial TGN retrieval in response to treatment with 50 μM $CuCl_2$ followed by treatment with 70 μM TTM (lower panel). C—The GFP-ATP7B-S1423N partially co-localizes with mKO2-ATP7B in response to 50 μM $CuCl_2$ treatment in the differentiated glia. D—Quantitation of the PCC of WT/ATP7B-S1423N and TGN38 ($n = 16$ under each condition). WT ATP7B and TGN38 show high PCC in the undifferentiated (0.48) and the differentiated (0.54), under basal condition demonstrating co-localization. WT ATP7B shows similar PCC value (0.49) as the basal condition upon TGN retrieval of ATP7B in presence of $CuCl_2$ followed by TTM treatment. ATP7B-S1423N and TGN38 show low PCC (0.08) demonstrating no co-localization between the markers in the undifferentiated C-6 cells. But the PCC value significantly increases (0.37) in the differentiated glia. The PCC value is lower (0.21) upon TGN retrieval ($CuCl_2$ + TTM), in the differentiated cells, compared to the basal condition. ****P-value < 0.0001. Images are captured by 63X oil immersion lens. Scale bar 5 μm.

suggest presence of unique interactions in the polarized and unpolarized system mediated through the C-terminus of ATP7B. Both S1423N and S1426I mutations have been identified in compound heterozygous form with L168P[17] and A1003V mutation,[19] respectively (Table 2). The compound heterozygote having S1423N mutation has mild neuropsychiatric symptoms. The milder symptoms can be contributed by the differences in the anterograde and retrograde trafficking behavior of the mutant. Alternatively, the milder symptoms can be a cumulative effect of the two mutations in compound heterozygous form. Future studies are warranted to provide an answer to these hypotheses. Again, T1434M is reported in compound heterozygous condition with the H1069Q[20] in the French population and with N1270S[16] in Costa Rican population (Table 2). The compound heterozygote in the Costa Rican population is designated as presymptomatic.[16] T1434M, in homozygous condition in an Egyptian patient, is associated with milder liver symptoms with no neurological manifestations[21] (Table 2). Milder liver symptoms and not severe ones might be due to the correction of the Cu(I) regulated trafficking, of the T1434M mutant, in the polarized systems like glia, MDCK and WIF-B.[15]

Our study suggests that the effects of S1423N, S1426I, and T1434M mutations are corrected (to varying extent) in the polarized/differentiated system. We hypothesize that the mutations, if detected in homozygous conditions, will lead to milder hepatic and neurological manifestations as the concerned organs consist majorly of polarized cells. WD, although monogenic, exhibits considerable phenotypic heterogeneity. One of the reasons for this heterogeneity is the differential effect of the mutations on ATP7B stability, which, in turn, dictates its cellular localization and function to a varying extent. Therefore, the treatment regime will largely be dictated by the severity of the individual mutations on the cellular phenotypes of ATP7B. The present study demonstrates

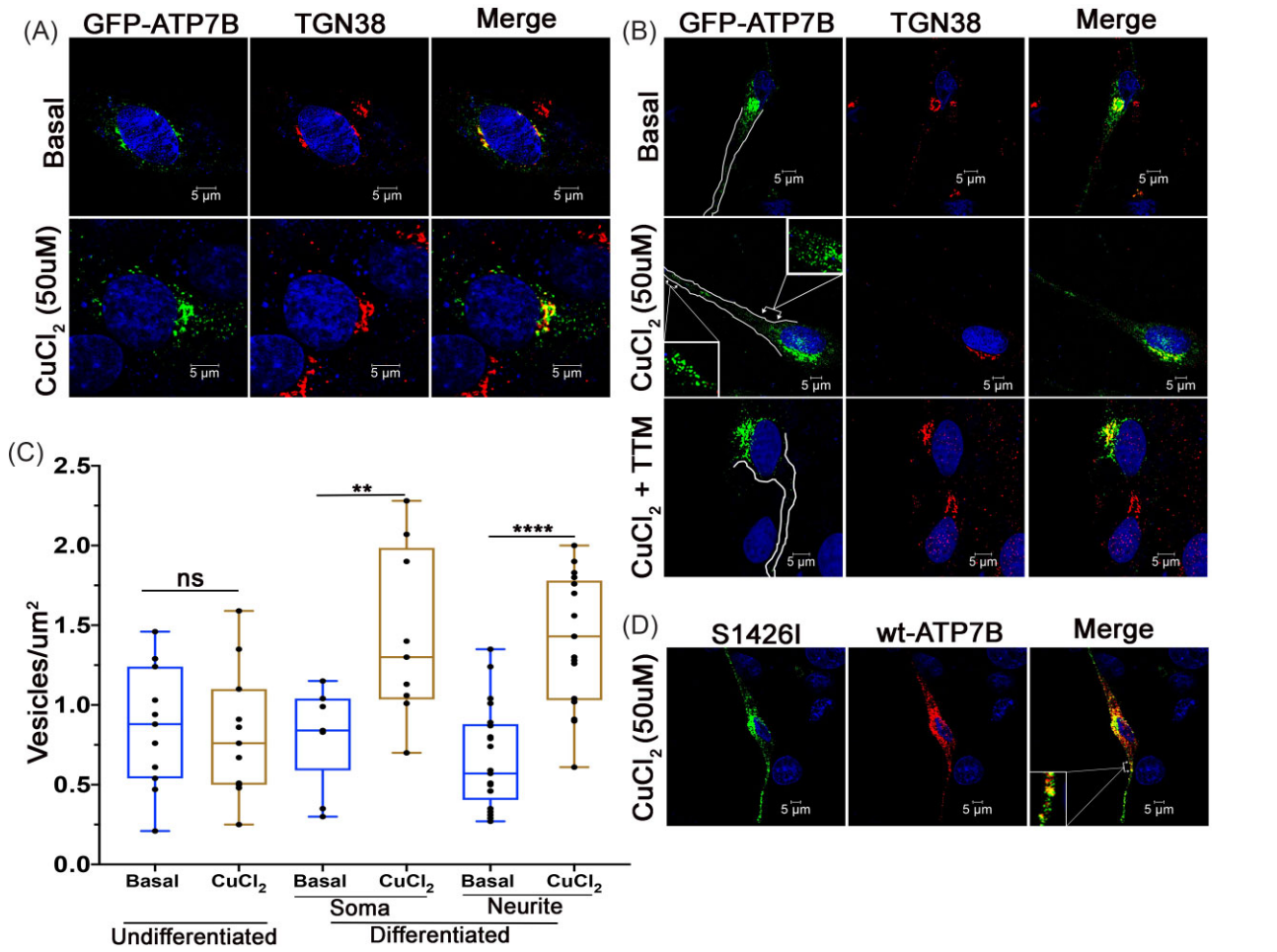

Fig. 11 Localization, anterograde and retrograde trafficking of ATP7B-S1426I in undifferentiated and differentiated (C-6 derived) glia. A—S1426I mutant localizes into the TGN in the undifferentiated C-6 cells (upper panel). However, the mutant cannot traffic to the vesicles in the undifferentiated C-6 cells (lower panel). B—The mutant localizes on TGN in the differentiated glia (upper panel) and can traffic to vesicles in response to treatment with 50 μM $CuCl_2$ treatment (middle). Inset—A portion of the soma and neurite has been magnified to demonstrate vesicles. The mutant can traffic back to the TGN in response to treatment with 50 μM $CuCl_2$ followed by 70 μM TTM (lower panel) treatment. C—Quantitation of vesicles/μm^2 has been represented. The mutant shows 0.86 vesicles/μm^2 ($n = 11$) under basal condition and 0.82 vesicles/μm^2 ($n = 11$) under $CuCl_2$ treatment in the undifferentiated C-6 cells. The mutant shows 0.82 vesicles/μm^2 ($n = 9$) under basal condition, which increases to 1.43 ($n = 9$) in response to $CuCl_2$ treatment in the soma region of the differentiated cells. Similarly, the mutant shows 0.66 vesicles/μm^2 ($n = 21$) in the neurite region under basal condition, which increases to 1.4 vesicles/μm^2 ($n = 17$) in response to $CuCl_2$ treatment. **P-value—0.0091, ****P-value<0.0001. D—Localization of GFP-ATP7B-S1426I and GFP-wt-ATP7B in response to 50 μM $CuCl_2$ treatment in the differentiated glia. A portion of the neurite has been magnified and demonstrated in the inset to demonstrate co-localization of mKO2-wt-ATP7B and GFP-ATP7B-S1426I on the vesicles.

that polarization of the cells also needs to be considered as an important factor that can modify the severity of a mutation. Efficient therapeutic strategy needs to include detection of the mutation and comprehensive study of its effects on the protein both in polarized and unpolarized cells with correlation to the phenotype.

As already mentioned, the present study highlights the importance of polarization of the cells as an important factor in determining the effect of the WD mutations on ATP7B. However, the study considers only cell-based model systems. Further studies are warranted to confirm the effects in organoid or organism-based model systems to better correlate the effects with phenotype. Such comprehensive understanding utilizing cell-based models to model organisms is needed to understand the effects of individual mutations. Such analysis will provide targeted therapeutic approaches with minimum side effects.

The C-terminal domain of ATP7B is present only in the eukaryotic copper transporters.[22] Probably, the C-terminus might have been acquired with the evolution of the organellar compartments, like the Golgi, in the eukaryotes. With the advent of the Golgi compartment, there arose the necessity to localize and traffic (both anterograde and retrograde) from the TGN to maintain cellular copper homeostasis. While the proximal region of the C-terminus (L1373-Q1399) affects ATP7B stability[7,23] (Table 2), the trileucine (LLL) (residues 1454–1456) at the distal end is essential for ATP7B's retrieval into the TGN.[15] But the role of the portion of the C-terminus between the proximal and the distal residues has never been highlighted. The WD mutations located in this region and their effect on ATP7B localization and function will shed light on the function of this region. S1423, S1426, and T1434 are the residues located in this region. The present study demonstrates that the residues are important for TGN localization and exit from the TGN in the unpolarized cells.

Insights from the structural studies provide ample indications of the C-terminus of ATP7B regulating the basal and copper-mediated localization of the protein. This is by the virtue of the interactions of the C-terminus with the cytosolic domains including

Table 2. C-Terminal mutations and their effect on cellular phenotypes

Mutations	Origin[a]		Cellular phenotypes	Detected as	Nature of the mutation	Patient phenotypes
	Geographical origin	Population				
L1373R	East Asia, Western Europe, South America	Japan, France, Brazil	Affects protein expression in MDCK-II and YS cells[7,15]	Heterozygous[26]	Missense	Mainly neurological manifestation with occasional hepatic symptoms
L1373P	East Asia	Japan	Affects protein expression in MDCK-II and YS cells[7,15]	Heterozygous[27]	Missense	Both hepatic and neurological symptoms[28]
C1375S	Eastern Europe	Ukraine,	Does not affect protein expression in YS cells[15]	Heterozygous[29]	Missense	
P1379S	Mediterranean	Italy	Adequate protein expression in YS cells[23]	Heterozygous[29]	Missense	
Q1399R	Middle East	Saudi Arabia	Affects Protein expression in YS cells[23]	Homozygous[30]	Missense	Neurological and/or hepatic symptoms
W1410X	Middle East, North Africa	Egypt	Does not affect protein expression in YS cells[23]	Homozygous[18]	Nonsense	
S1423N	Central Europe	Germany	Does not affect any protein expression in polarized MDCK-II cells[23]	Compound heterozygous with L168P[17]	Missense	Mild neuropsychiatric symptoms; the patient also has Gilbert syndrome (p.TA7/7 mutation in *UGT1A1*)
S1426I	South Asia	India	Does not affect protein expression in HEK293 cells[10]	Compound heterozygous with A1003V[19]	Missense	
T1434M	Mediterranean, Middle East, North Africa	Italy, Egypt	Does not affect protein expression in HEK293 cells (Present study and[23])	Compound heterozygous with N1270S[16, 18] and homozygous form[21]	Missense	Both neurological and hepatic manifestations with some patients exhibiting chronic liver disease
X1466R	[b]Central Europe and South-Eastern Europe	[b]Romania, Greece	Does not affect protein expression in YS cells	Compound heterozygous with H1069Q[31] and homozygous form[32]	Missense	Hepatic symptoms including acute liver failure

Note: [a]The data in the Origin Column have been derived from WilsonGen website maintained by IGIB (Institute of Genome and Integrative Biology) https://clingen.igib.res.in/WilsonGen/
[b]Not included in the WilsonGen website and based upon the literature.

the N-terminus.[22] It is probable that the distal C-terminal mutations (S1423N, S1426I, and T1434M) can affect the local topology of the domain, which can affect its interaction with other domains as well as with other proteins thereby affecting the unique interactions in the unpolarized system. P1386S mutation in ATP7A has been demonstrated to cause topological change thereby affecting the membrane insertion of the eighth transmembrane segment of ATP7A causing distal motor neuropathy.[24,25] The C-terminal WD mutations, in the present study, have provided important information on the role of this domain in TGN localization and exit. This might dictate both copper transport into the TGN and copper export functions of ATP7B. Future in-depth studies are needed to fully unravel the role of the C-terminus and the WD mutations will serve as an important tool towards understanding such mechanisms.

Supplementary material

Supplementary data are available at *Metallomics* online.

Funding

The study is supported by the Ramanujan Fellowship Project (SB/S2/RJN-106/2015) and Extramural Research Project (EMR/2016/003293) to A.B. from the Science and Engineering Research Board (SERB), Department of Science and Technology (DST), Government of India. Further, Wellcome Trust India Alliance Fellowship (IA/I/16/1/502369) and Core Research Grant (CRG/2021/002150) from SERB, DST, Government of India to A.G. is gratefully acknowledged. K.C. is supported by the Indian Council of Medical Research-Senior Research Fellowship (ICMR-SRF, 2020-7142/CMB-BMS).

Author contributions

A.B. conceived the study plan. K.C., S.D., A.P., S.M., and B.R. performed the experiments and procured data. A.B., K.C., and A.G. have planned the experiments and analysed the data. A.B., K.C., and A.G. wrote the manuscript.

Conflict of interest

The authors declare that they have no conflicts of interest with the contents of this article.

Data availability

The authors ensure that the manuscript contains all the required data. The datasets that are represented in the manuscript do not contain any software codes that need to be archived.

References

1. A. Członkowska, T. Litwin, P. Dusek, P. Ferenci, S. Lutsenko, V. Medici, J. K. Rybakowski, K. H. Weiss and M. L. Schilsky, Wilson Disease, *Nat. Rev. Dis. Primers*, 2018, 4 (1), 21. https://doi.org/10.1038/s41572-018-0018-3
2. M. Schushan, A. Bhattacharjee, N. Ben-Tal and S. Lutsenko, A Structural Model of the Copper ATPase ATP7B to Facilitate Analysis of Wilson Disease-Causing Mutations and Studies of the Transport Mechanism, *Metallomics Integr. Biomet. Sci.*, 2012, 4 (7), 669–678. https://doi.org/10.1039/c2mt20025b
3. S. Lutsenko, A. Gupta, J. L. Burkhead and V. Zuzel, Cellular Multitasking: the Dual Role of Human Cu-ATPases in Cofactor Delivery and Intracellular Copper Balance, *Arch. Biochem. Biophys.*, 2008, 476 (1), 22–32. https://doi.org/10.1016/j.abb.2008.05.005
4. M. Varadi, S. Anyango, M. Deshpande, S. Nair, C. Natassia, G. Yordanova, D. Yuan, O. Stroe, G. Wood, A. Laydon, A. Žídek, T. Green, K. Tunyasuvunakool, S. Petersen, J. Jumper, E. Clancy, R. Green, A. Vora, M. Lutfi, M. Figurnov, A. Cowie, N. Hobbs, P. Kohli, G. Kleywegt, E. Birney, D. Hassabis and S. Velankar, AlphaFold Protein Structure Database: Massively Expanding the Structural Coverage of Protein-Sequence Space with High-Accuracy Models, *Nucleic Acids Res.*, 2022, 50 (D1), D439–D444. https://doi.org/10.1093/nar/gkab1061
5. J. Jumper, R. Evans, A. Pritzel, T. Green, M. Figurnov, O. Ronneberger, K. Tunyasuvunakool, R. Bates, A. Žídek, A. Potapenko, A. Bridgland, C. Meyer, S. A. A. Kohl, A. J. Ballard, A. Cowie, B. Romera-Paredes, S. Nikolov, R. Jain, J. Adler, T. Back, S. Petersen, D. Reiman, E. Clancy, M. Zielinski, M. Steinegger, M. Pacholska, T. Berghammer, S. Bodenstein, D. Silver, O. Vinyals, A. W. Senior, K. Kavukcuoglu, P. Kohli and D. Hassabis, Highly Accurate Protein Structure Prediction with AlphaFold, *Nature*, 2021, 596 (7873), 583–589. https://doi.org/10.1038/s41586-021-03819-2
6. K. Chakraborty, S. Kar, B. Rai, R. Bhagat, N. Naskar, P. Seth, A. Gupta and A. Bhattacharjee, Copper Dependent ERK1/2 Phosphorylation Is Essential for the Viability of Neurons and Not Glia, *Metallomics Integr. Biomet. Sci.*, 2022, 14 (4). https://doi.org/10.1093/mtomcs/mfac005
7. S. Das, A. Mohammed, T. Mandal, S. Maji, J. Verma, Ruturaj and A. Gupta, Polarized Trafficking and Copper Transport Activity of ATP7B: a Mutational Approach to Establish Genotype-Phenotype Correlation in Wilson Disease, *Hum. Mutat.*, 2022, 43 (10), 1408–1429. https://doi.org/10.1002/humu.24428
8. O. Y. Dmitriev, A. Bhattacharjee, S. Nokhrin, E. M. Uhlemann and S. Lutsenko, Difference in Stability of the N-Domain Underlies distinct Intracellular Properties of the E1064A and H1069Q Mutants of Copper-Transporting ATPase ATP7B, *J. Biol. Chem.*, 2011, 286 (18), 16355–16362. https://doi.org/10.1074/jbc.M110.198101
9. A. Gupta, M. Maulik, P. Nasipuri, I. Chattopadhyay, S. K. Das, P. K. Gangopadhyay and K. Ray, Molecular Diagnosis of Wilson Disease using Prevalent Mutations and Informative Single-Nucleotide Polymorphism Markers, *Clin. Chem.*, 2007, 53 (9), 1601–1608. https://doi.org/10.1373/clinchem.2007.086066
10. S. Roy, C. J. McCann, M. Ralle, K. Ray, J. Ray, S. Lutsenko and S. Jayakanthan, Analysis of Wilson Disease Mutations Revealed that Interactions between Different ATP7B Mutants Modify Their Properties, *Sci. Rep.*, 2020, 10 (1), 13487. https://doi.org/10.1038/s41598-020-70366-7
11. L. T. Braiterman, A. Murthy, S. Jayakanthan, L. Nyasae, E. Tzeng, G. Gromadzka, T. B. Woolf, S. Lutsenko and A. L. Hubbard, Distinct Phenotype of a Wilson Disease Mutation Reveals a Novel Trafficking Determinant in the Copper Transporter ATP7B, *Proc. Nat. Acad. Sci. U.S.A.*, 2014, 111, E1364–E1373.
12. M. J. Petris, D. Strausak and J. F. Mercer, The Menkes Copper Transporter Is Required for the Activation of Tyrosinase, *Hum. Mol. Genet.*, 2000, 9 (19), 2845–2851. https://doi.org/10.1093/hmg/9.19.2845
13. S. A. K. Wilson, Progressive Lenticular Degeneration: a Familial Nervous Disease Associated with Cirrhosis of the Liver, *Brain*, 1912, 34 (4), 295–507. https://doi.org/10.1093/brain/34.4.295
14. S. K. Das and K. Ray, Wilson's Disease: an Update, *Nat. Rev. Neurol.*, 2006, 2 (9), 482–493. https://doi.org/10.1038/ncpneuro0291
15. L. Braiterman, L. Nyasae, F. Leves and A. L. Hubbard, Critical Roles for the COOH Terminus of the Cu-ATPase ATP7B in

Protein Stability, Trans-Golgi Network Retention, Copper Sensing, and Retrograde Trafficking, *Am. J. Physiol. –Gastrointest. Liver Physiol.*, 2011, 301 (1), G69–G81. https://doi.org/10.1152/ajpgi.00038.2011
16. M. Penon-Portmann, S. Lotz-Esquivel, A. Chavez Carrera, M. Jiménez-Hernández, D. Alvarado-Romero, S. Segura-Cordero, F. Rimolo-Donadio, F. Hevia-Urrutia, A. Mora-Guevara, M. Saborío-Rocafort, G. Jiménez-Arguedas and R. Badilla-Porras, Wilson Disease in Costa Rica: Pediatric Phenotype and Genotype Characterization, *JIMD Rep.*, 2020, 52 (1), 55–62. https://doi.org/10.1002/jmd2.12098
17. S. Guttmann, F. Bernick, M. Naorniakowska, U. Michgehl, S. R. Groba, P. Socha, A. Zibert and H. H. Schmidt, Functional Characterization of Novel ATP7B Variants for Diagnosis of Wilson Disease, *Front. Pediatr.*, 2018, 6, 106. https://doi.org/10.3389/fped.2018.00106
18. T. Y. Abdelghaffar, S. M. Elsayed, E. Elsobky, B. Bochow, J. Büttner and H. Schmidt, Mutational Analysis of ATP7B gene in Egyptian Children with Wilson Disease: 12 Novel Mutations, *J. Hum. Genet.*, 2008, 53 (8), 681. https://doi.org/10.1007/s10038-008-0298-7
19. S. Mukherjee, S. Dutta, S. Majumdar, T. Biswas, P. Jaiswal, M. Sengupta, A. Bhattacharya, P. K. Gangopadhyay, A. Bavdekar, S. K. Das and K. Ray, Genetic Defects in Indian Wilson Disease Patients and Genotype-Phenotype Correlation, *Parkinsonism Relat. Disord.*, 2014, 20, 75–81.
20. C. Demily, F. Parant, D. Cheillan, E. Broussolle, A. Pavec, O. Guillaud, L. Restier, A. Lachaux and M. Bost, Screening of Wilson's Disease in a Psychiatric Population: Difficulties and Pitfalls. A Preliminary Study, *Ann. Gen. Psych.*, 2017, 16 (1), 19. https://doi.org/10.1186/s12991-017-0142-6
21. T. Y. Abdel Ghaffar, S. M. Elsayed, S. Elnaghy, A. Shadeed, E. S. Elsobky and H. Schmidt, Phenotypic and Genetic Characterization of a Cohort of Pediatric Wilson Disease Patients, *BMC Pediatr.*, 2011, 11 (1), 56. https://doi.org/10.1186/1471-2431-11-56
22. R. M. Bitter, S. Oh, Z. Deng, S. Rahman, R. K. Hite and P. Yuan, Structure of the Wilson Disease Copper Transporter ATP7B, *Sci. Adv.*, 2022, 8 (9), eabl5508. https://doi.org/10.1126/sciadv.abl5508
23. L. T. Braiterman, A. Gupta, R. Chaerkady, R. N. Cole and A. L. Hubbard, Communication between the N and C Termini Is Required for Copper-Stimulated Ser/Thr Phosphorylation of Cu(I)-ATPase (ATP7B), *J. Biol. Chem.*, 2015, 290 (14), 8803–8819. https://doi.org/10.1074/jbc.M114.627414
24. L. Yi and S. G. Kaler, Direct Interactions of Adaptor Protein Complexes 1 and 2 with the Copper Transporter ATP7A Mediate Its Anterograde and Retrograde Trafficking, *Hum. Mol. Genet.*, 2015, 24 (9), 2411–2425. https://doi.org/10.1093/hmg/ddv002
25. L. Yi, A. Donsante, M. L. Kennerson, J. F. Mercer, J. Y. Garbern and S. G. Kaler, Altered Intracellular Localization and Valosin-Containing Protein (p97 VCP) Interaction Underlie ATP7A-Related Distal Motor Neuropathy, *Hum. Mol. Genet.*, 2012, 21 (8), 1794–1807. https://doi.org/10.1093/hmg/ddr612
26. M. M. Deguti, J. Genschel, E. L. Cancado, E. R. Barbosa, B. Bochow, M. Mucenic, G. Porta, H. Lochs, F. J. Carrilho and H. H. Schmidt, Wilson Disease: Novel Mutations in the ATP7B Gene and Clinical Correlation in Brazilian Patients, *Hum. Mutat.*, 2004, 23 (4), 398. https://doi.org/10.1002/humu.9227
27. T. Okada, Y. Shiono, H. Hayashi, H. Satoh, T. Sawada, A. Suzuki, Y. Takeda, M. Yano, K. Michitaka, M. Onji and H. Mabuchi, Mutational Analysis of ATP7B and Genotype-Phenotype Correlation in Japanese with Wilson's Disease, *Hum. Mutat.*, 2000, 15 (5), 454–462. https://doi.org/10.1002/(SICI)1098-1004(200005)15:5%3c454::AID-HUMU7%3e3.0.CO;2-J
28. A. Gupta, S. Das and K. Ray, A Glimpse into the Regulation of the Wilson Disease Protein, ATP7B, Sheds Light on the Complexity of Mammalian Apical Trafficking Pathways, *Metallomics*, 2018, 10 (3), 378–387. https://doi.org/10.1039/C7MT00314E
29. D. W. Cox, L. Prat, J. M. Walshe, J. Heathcote and D. Gaffney, Twenty-Four Novel Mutations in Wilson Disease Patients of Predominantly European Ancestry, *Hum. Mutat.*, 2005, 26 (3), 280. https://doi.org/10.1002/humu.9358
30. M. Al Jumah, R. Majumdar, S. Al Rajeh, A. Awada, A. Al Zaben, I. Al Traif, A. R. Al Jumah and Z. Rehana, A Clinical and Genetic Study of 56 Saudi Wilson Disease Patients: Identification Of Saudi-Specific Mutations, *Eur. J. Neurol.*, 2004, 11, 121–124.
31. P. Butler, N. McIntyre and P. K. Mistry, Molecular Diagnosis of Wilson Disease, *Mol. Genet. Metab.*, 2001, 72 (3), 223–230. https://doi.org/10.1006/mgme.2000.3143
32. G. Loudianos, M. Lovicu, P. Solinas, E. Kanavakis, M. Tzetis, N. Manolaki, E. Panagiotakaki, T. Karpathios and A. Cao, Delineation of the Spectrum of Wilson Disease Mutations in the Greek Population and the Identification of Six Novel Mutations, *Genet. Test.*, 2000, 4 (4), 399–402. https://doi.org/10.1089/109065700750065162

Received: March 22, 2023. **Accepted:** August 6, 2023